THE JOURNAL OF PHYSICAL CHEMISTRY A

Article

Cite This: J. Phys. Chem. A 2019, 123, 7087−7103

pubs.acs.org/JPCA

Interplay of Ring Puckering and Hydrogen Bonding in Deoxyribonucleosides

Published as part of The Journal of Physical Chemistry virtual special issue "Leo Radom Festschrift".

Siying Lyu,‡ Nassim Beiranvand,‡ Marek Freindorf, and Elfi Kraka*

Computational and Theoretical Chemistry Group (CATCO), Department of Chemistry, Southern Methodist University, 3215 Daniel Ave, Dallas, Texas 75275-0314, United States

Supporting Information

ABSTRACT: The Cremer−Pople ring puckering analysis and the Konkoli−Cremer local mode analysis supported by the topological analysis of the electron density were applied for the first comprehensive analysis of the interplay between deoxyribose ring puckering and intramolecular H-bonding in 2′-deoxycytidine, 2′-deoxyadenosine, 2′-deoxythymidine, and 2′-deoxyguanosine. We mapped for each deoxyribonucleoside the complete conformational energy surface and the corresponding pseudorotation path. We found only incomplete pseudorotation cycles, caused by ring inversion, which we coined as pseudolibration paths. On each pseudolibration path a global and a local minimum separated by a transition state were identified. The investigation of H-bond free deoxyribonucleoside analogs revealed that removal of the H-bond does not restore the full conformational flexibility of the sugar ring. Our work showed that ring puckering predominantly determines the conformational energy; the larger the puckering amplitude, the lower the conformational energy. In contrast no direct correlation between conformational energy and H-bond strength was found. The longest and weakest H-bonds are located in the local minimum region, whereas the shortest and strongest H-bonds are located outside the global and local minimum regions at the turning points of the pseudolibration paths, i.e., H-bonding determines the shape and length of the pseudolibration paths. In addition to the H-bond strength, we evaluated the covalent/electrostatic character of the H-bonds applying the Cremer−Kraka criterion of covalent bonding. H-bonding in the puric bases has a more covalent character whereas in the pyrimidic bases the H-bond character is more electrostatic. We investigated how the mutual orientation of the CH_2OH group and the base influences H-bond formation via two geometrical parameters describing the rotation of the substituents perpendicular to the sugar ring and their tilting relative to the ring center. According to our results, rotation is more important for H-bond formation. In addition we assessed the influence of the H-bond acceptor, the lone pair (N, respectively O), via the delocalization energy. We found larger delocalization energies corresponding to stronger H-bonds for the puric bases. The global minimum conformation of 2′-deoxyguanosine has the strongest H-bond of all conformers investigated in this work with a bond strength of 0.436 which is even stronger than the H-bond in the water dimer (0.360). The application of our new analysis to DNA deoxyribonucleotides and to unnatural base pairs, which have recently drawn a lot of attention, is in progress.

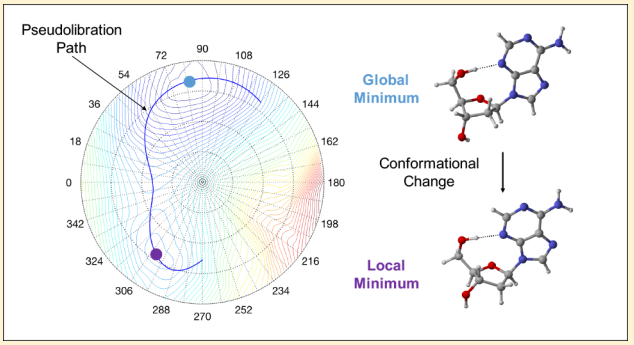

INTRODUCTION

Deoxyribonucleosides and their analogs are important building blocks for the synthesis of antiviral drugs and anticancer agents,[1−3] and the production of deoxyribonucleotides for polymerase chain reactions.[4−6] They can serve as biological probes.[7] Certain bacteria, e.g., the Gram-positive soil bacterium *Bacillus subtilis*, can utilize deoxyribonucleosides via the catabolic deoxyribonucleoside pathway as a sources of carbon and energy.[8] The reverse deoxyriboaldolase enzyme (DERA)[9] can drive the deoxyribonucleoside synthesis showing great promise for industrial-scale production of deoxyribonucleosides.[10,11] The DERA pathway has recently attracted a lot of attention as a possible alternative to the production of deoxyribonucleotides via ribonucleotide reductases (RNRs).[9,12] Therefore, understanding more about deoxyribonucleosides and their synthesis via the DERA pathway offers an important gateway to new mechanistic insights into this pathway, which could help us to understand the suggested DERA production of deoxyribonucleotides shedding more light onto the origin of DNA.[12] One important ingredient along this route is to understand the conformational flexibility of deoxyribonucleosides, which is determined by a complex

Received: June 7, 2019
Revised: July 19, 2019
Published: July 19, 2019

DOI: 10.1021/acs.jpca.9b05452
J. Phys. Chem. A 2019, 123, 7087−7103

interplay of ring puckering of the deoxyribose sugar ring and intramolecular hydrogen bonding (H-bonding). So far, conformational studies of deoxyribonucleosides have focused mostly on either the ring puckering or the H-bonding aspect. In 1972, Altona and Sundaralingam[13] introduced a procedure describing both the puckering angle and puckering amplitude of a five-membered ring via torsional angles. However, the definition of the ring puckering amplitude expressed via an angle does not allow the appropriate description of the ring pseudorotation process. In this process, the maximum puckering amplitude is rotating around the edge of the ring without raising a substantial potential energy change. Such a movement can be best described with a puckering amplitude defined as displacement from a reference. Ring puckering and pseudorotation of nucleosides based on the Altona and Sundaralingam approach were able to describe the molecular properties of specific deoxyribose sugar ring conformations; however, they failed to describe the changes of molecular properties along the pseudorotation path in a smooth form.[2,14−17] Other studies focused on the influence of the intramolecular hydrogen bonds (H-bond)s on the conformational of deoxyribonucleosides.[18−23] They investigated predominantly the internal H-bonds between the base and the CH_2OH group of the sugar ring. Other internal H-bonds resulting from a rotation of the base unit were not considered in a systematic fashion. Studies of the correlation between ring puckering and H-bonding have been rarely reported, even when the conformational energy surface (CES) was explored,[24] or when global reactivity parameters were derived.[2]

Therefore, the way that deoxyribose ring puckering affects the formation of internal H-bonding and vice versa is not fully understood yet. To understand the driving force of the conformational flexibility of deoxyribonucleosides it is important (i) to quantitatively assess both, ring puckering and H-bonding, and (ii) to investigate the relationship between these two essential structural features. We used in this work as an efficient tool a combination of the Cremer−Pople *ring puckering analysis*[25−30] and the *local mode analysis* of Konkoli and Cremer,[31−34] which describes the conformational process at the quantum mechanical level. In particular, the following objectives were included in our study:

- To exploit the CES, to determine the pseudorotation path and the location of the global and local minima on the CES for the deoxyribonucleosides **dC**, **dA**, **dT**, and **dG**; see Figure 1.
- To investigate how the conformational energy, the puckering amplitude, and the H-bond properties such as distance and bond strength change along the pseudorotation path of deoxyribose ring and how these changes are connected; as an important step to understand the interplay between sugar ring puckering and H-bonding.
- To monitor the change of the covalent character of the H-bonds along the pseudorotation path via the topological analysis of the electron density.

The paper is structured in the following way. In the second section the methods used in this work are described as well as computational details. The third section presents the results and discussion. Conclusions and an outlook are made in the final section.

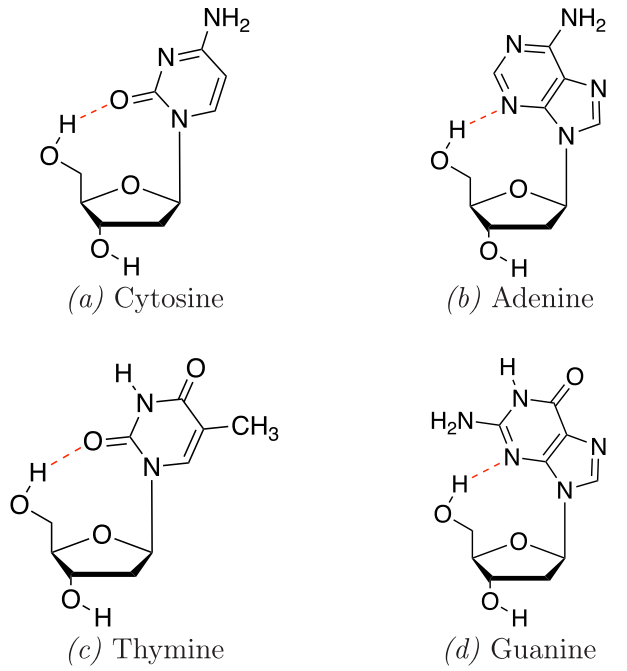

Figure 1. Deoxyribonucleosides investigated in this work: (a) 2′-deoxycytidine (cytosine), **dC**, (b) 2′-deoxyadenosine (adenine), **dA**, (c) thymidine (thymine), **dT**, (d) 2′-deoxyguanosine (guanine), **dG**. The red dashed line indicates the internal H-bond between the base and the CH_2OH substituent of the sugar ring.

METHODOLOGIES

In this section, the important tools applied in this work are introduced, the Cremer−Pople ring puckering analysis,[25−30] the local mode analysis of Konkoli and Cremer,[31−34] and the topological analysis of the electron density $\rho(r)$ via Bader's quantum theory of atoms in molecules (QTAIM) approach.[35,36] Then the computational details of this study are described.

Cremer−Pople Ring Puckering Analysis. Cremer and Pople[25] suggested to span the conformational space of a puckered N-membered ring with $N - 3$ puckering coordinates. The $N - 3$ puckering coordinates can be split up into pairs of pseudorotational coordinates $\{q_m, \phi_m\}$ ($m = 2, 3, ..., N - 3$) for odd-membered rings and an additional puckering amplitude $q_{N/2}$ describing ring inversion for even-membered rings. The puckering amplitude q_m describes the degree of ring puckering of the mth puckering mode. The puckering angle ϕ_m defines ring puckering mode.[37,38] Cremer and Pople[25] introduced a mean plane as reference, e.g. the plane of the planar ring. The out-of-plane coordinates z_j, describing the displacement perpendicular to the mean plane can be determined by the $N - 3$ puckering coordinate pairs $\{q_m, \phi_m\}$.[25,37,39−41] For a five-membered ring with ring atoms $j = 1, ..., 5$, the out-of-plane displacements z_j for any ring conformation are given by eq 1:[25,42]

$$z_j = \left(\frac{2}{5}\right)^{1/2} q_2 \cos\left[\frac{4\pi(j-1)}{5} + \phi_2\right] \quad \text{for } j = 1, ..., 5 \text{ and } \phi_2 \in [0; 2\pi] \tag{1}$$

where the displacement z_j coordinates are normalized according to

DOI: 10.1021/acs.jpca.9b05452
J. Phys. Chem. A 2019, 123, 7087−7103

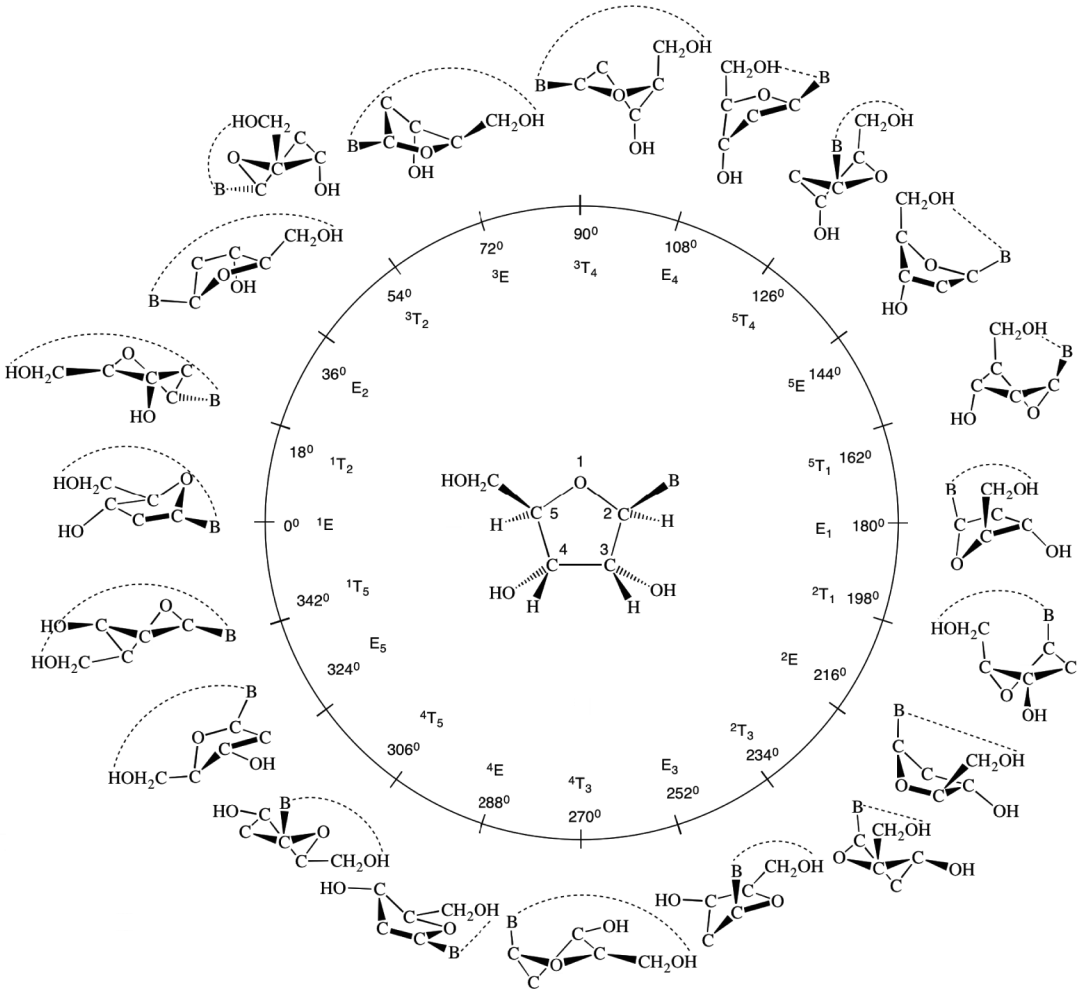

Figure 2. Pseudorotational cycle ($\phi_2 = 0° \rightarrow 360°$) of the deoxyribonucleoside sugar-ring represented by 20 conformers, (10 envelope (E) forms, $\phi_2 = (0 + 360k)/10$ and 10 twist (T) forms $\phi_2 = (18 + 360k)/10$, where $k = 0, 1, 2, ..., 9$). The planar form is located at the center ($q_2 = 0$ Å). The symbol B represents the base of the deoxyribonucleoside. The dashed line indicates the internal H-bond between the base and the CH_2OH substituent of the sugar ring.

$$\sum_{j=1}^{5} z_j^2 = q_2^2 \tag{2}$$

Using puckering coordinates, the full set of $3N - 6$ independent Cartesian coordinates of any puckered N-membered ring can be uniquely determined via $N - 3$ puckering coordinates (q and ϕ), $N - 3$ bond angles, and N bond lengths. Besides the out-of-plane displacement z_j, the displacements in the perpendicular x_j and y_j directions can also be specified. First, the z_j coordinates are calculated according to eq 1 (or similar formulas for $N > 5$);[39,42] then, the N bond lengths and $N - 3$ bond angles are projected onto the mean plane of the ring. Finally, the projected ring is partitioned into segments, for which the displacements x_j and y_j are calculated according to a procedure described by Cremer.[25]

Although there is an infinite number of ring conformations located on a pseudorotation cycle for the sugar ring of deoxyribonucleosides, it is sufficient to investigate a representative number of conformations, as shown in Figure 2. Referring to previous work on description of tetrahydrofuran,[42] which is an analog to the five-membered sugar ring in deoxyribose, a subset of 20 ring conformations were optimized using a mixed set of puckering and internal coordinates. As shown in Figure 2, there are 10 envelope (E) forms located at $\phi_2 = (0 + 360k)/10$ (for $k = 0, 1, 2, ..., 9$) and 10 twist forms located at $\phi_2 = (18 + 360k)/10$ (for $k = 0, 1, 2, ..., 9$). The internal H-bonds between the base and CH_2OH group of the sugar ring are indicated by a dashed line. The ring atom, which lies above the mean plane, is noted in front of the conformational symbol E/T as superscript, whereas a ring atom, which lies below the mean plane, is noted after the symbol E/T as subscript. All deoxyribonucleosides considered in this work possess C_1 symmetry; therefore, the CES must also have C_1 symmetry.

There are two major advantages of using ring puckering coordinates.[43,44] First, the geometry of the sugar ring for any given value of q_2 and ϕ_2 can be optimized, even if this conformation does not occupy a stationary point on the CES. This would not be feasible by a description of the ring with Cartesian or internal coordinates.[30] For substituted ring systems such as deoxyribonucleosides, any conformer located on the CES can be uniquely described by a mixed set of puckering coordinates for the ring and internal/Cartesian coordinates for the substituents, and a physically meaningful pseudorotation path as a function of ϕ_2 can be obtained. The second advantage is that any property P of a puckered ring, such as energy, geometry, dipole moment, charge distribution, vibrational frequencies, or magnetic properties, can be expressed as a

DOI: 10.1021/acs.jpca.9b05452
J. Phys. Chem. A 2019, 123, 7087−7103

Fourier series of the puckering coordinates. In the case of a five-membered ring, P takes the following general form:[42]

$$P(q_2, \phi_2) = \sum_{k=0}^{\infty} [P_k^c(q_2)\cos(k\phi_2) + P_k^s(q_2)\sin(k\phi_2)] \quad (3)$$

where the Fourier coefficients P_k^c and P_k^s are in turn expressed as power series in the puckering amplitude q_2:[42]

$$P_k(q_2) = \sum_{l=0}^{\infty} P_{kl} q_2^l \quad (4)$$

Depending on the symmetry of the ring, eq 3 can be simplified by selecting trigonometric terms. Because the puckering amplitude as well as the coefficients P_{kl} change independent of the phase angle ϕ_2, the puckering amplitude q_2 the Fourier coefficients can be treated as normal coefficients for further simplification. Thus, the property P can be expressed as a pure function of ϕ_2, which also holds for the change of a property P along the pseudorotation path. For C_1 symmetric systems eq 3 can be simplified to eq 5, which was applied in this work:

$$P(\phi_2) = \sum_{k=0}^{\infty} (A_k\cos(k\phi_2) + B_k\sin(k\phi_2)) \quad (5)$$

which according to the C_1 symmetry of the deoxyribonucleosides **dC**, **dA**, **dT**, and **dG**, investigated in this work leads to

$$P(\phi_2) = A_0 + \sum_{i=1}^{\infty}\left(A_i\cos(i\phi_2) + \sum_{j=1}^{\infty} B_j\sin(j\phi_2)\right) \quad (6)$$

Experimentally, for a free or slightly hindered pseudorotor molecule, only a property $\langle P\rangle$ averaged over all pseudorotational modes can be measured. Focusing exclusively on the large amplitude pseudorotational mode of the ring, the calculated property $\langle P\rangle$ averaged over the pseudorotational motion can be determined, once the functional form of eq 6 is known, according to[42]

$$\langle P\rangle = \int_b^a \rho(\phi_2)P(\phi)\,\mathrm{d}\phi_2 \quad (7)$$

where a and b are the boundary of pseudorotation. If $a \neq 2\pi$ and $b \neq 0$, the pseudorotation is incomplete, which we call pseudolibration in reference to physics calling an incomplete rotation a libration.

The conformational probability distribution $\rho(\phi_2)$ can be defined as a Boltzmann distribution:

$$\rho(\phi_2) = \frac{e^{-[V(\phi_2)-V(0)]/RT}}{\int_b^a e^{-[V(\phi_2)-V(0)]/RT}\,\mathrm{d}\phi_2} \quad (8)$$

where $V(\phi_2)$ is the electronic potential energy of the conformer at ϕ_2 on the pseudorotation path and $V(0)$ is the electronic potential energy of planar form. The conformational probability distribution $\rho(\phi_2)$ can be treated as a property P and, therefore, can be defined using eq 9:

$$\rho(\phi_2) = C_0 + \sum_{i=1}^{\infty}\left(C_i\cos(i\phi_2) + \sum_{j=1}^{\infty} D_j\sin(j\phi_2)\right) \quad (9)$$

The conformational probability distribution $\rho(\phi_2)$ reflects the most likely conformers of a puckered ring on the CES.

Local Mode Analysis. The normal $(3N - L)$ vibrational modes of an N atomic molecule (L is the number of translational and rotational motions of the molecule) contain important electronic structure information and, therefore, should be well suited as a measure of bond strength. However, it is difficult to decode this information into individual atom−atom interactions (e.g., those resulting in bonding) because normal vibrational modes are generally delocalized due to the coupling of the motions of the atoms within the molecule. There are two different coupling mechanisms between vibrational modes as a consequence of the fact that there is a kinetic and a potential contribution to the energy of a vibrational mode, as reflected in the corresponding Euler−Lagrange equations $L(\mathbf{q}, \dot{\mathbf{q}})$ for a vibrating molecule given by eq 10 in internal coordinates $\mathbf{q}$:[31−34]

$$L(\mathbf{q}, \dot{\mathbf{q}}) = \underbrace{\frac{1}{2}\dot{\mathbf{q}}^{\dagger}\mathbf{G}^{-1}\dot{\mathbf{q}}}_{\text{mass coupling}} - \underbrace{\frac{1}{2}\dot{\mathbf{q}}^{\dagger}\mathbf{F}^{q}\mathbf{q}}_{\text{electronic coupling}} \quad (10)$$

The electronic coupling between the vibrational modes is reflected by the off-diagonal elements of the force constant matrix $\mathbf{F}^q$. By solving the Euler−Lagrange equations for a vibrating molecule, the basic equation of vibrational spectroscopy, e.g. the Wilson equation,[45] is obtained:

$$\mathbf{F}^{\mathbf{q}}\mathbf{D} = \mathbf{G}^{-1}\mathbf{D}\boldsymbol{\Lambda} \quad (11)$$

with the diagonal matrix $\boldsymbol{\Lambda}$ collecting the vibrational eigenvalues $\lambda_\mu = 4\pi^2c^2\omega_\mu$ where ω_μ represents the harmonic vibrational frequency of mode $\mathbf{d}_\mu$ given in reciprocal centimeters, c is the speed of light, and $\mu = (1\cdots N - L)$. Solution of eq 11, e.g. diagonalizing the Wilson equation leads to the diagonal force constant $\mathbf{K}$ given in normal coordinates $\mathbf{Q}$ which is free of electronic coupling:

$$\mathbf{K} = \mathbf{D}^{\dagger}\mathbf{F}^{\mathbf{q}}\mathbf{D} \quad (12)$$

Kinematic coupling or mass coupling is still present when the electronic coupling is eliminated by solving the Wilson equation. In 1998, Konkoli and Cremer[31−34] determined for the first time local, mass-decoupled vibrational modes $\mathbf{a}_i$ directly from normal vibrational modes $\mathbf{d}_\mu$ by solving the mass-decoupled Euler−Lagrange equations. The subscript i specifies an internal coordinate q_i and the local mode is expressed in terms of normal coordinates $\mathbf{Q}$ associated with force constant matrix $\mathbf{K}$ of eq 12. Konkoli and Cremer showed that this is equivalent to requiring an adiabatic relaxation of the molecule after enforcing a local displacement of atoms by changing a specific internal coordinate as, e.g., a bond length (*leading parameter principle*).[31] The local modes are unique and the local counterparts of the normal vibrational modes. They can be based on either calculated or experimentally determined vibrational frequencies via[31−34,46−48]

$$\mathbf{a}_i = \frac{\mathbf{K}^{-1}\mathbf{d}_i^{\dagger}}{\mathbf{d}_i\mathbf{K}^{-1}\mathbf{d}_i^{\dagger}} \quad (13)$$

To each local mode $\mathbf{a}_i$ a corresponding local mode frequency ω_i^a, local mode mass $G_{i,i}^a$, and a local force constant k_i^a can be defined.[31] The local mode frequencies can be uniquely connected to the normal-mode frequencies via an adiabatic connection scheme.[33,34] The local mode frequency ω_i^a is defined by

$$(\omega_i^a)^2 = \frac{G_{i,i}^a k_i^a}{4\pi^2c^2} \quad (14)$$

and the corresponding local mode force constant k_i^a by

DOI: 10.1021/acs.jpca.9b05452
J. Phys. Chem. A 2019, 123, 7087−7103

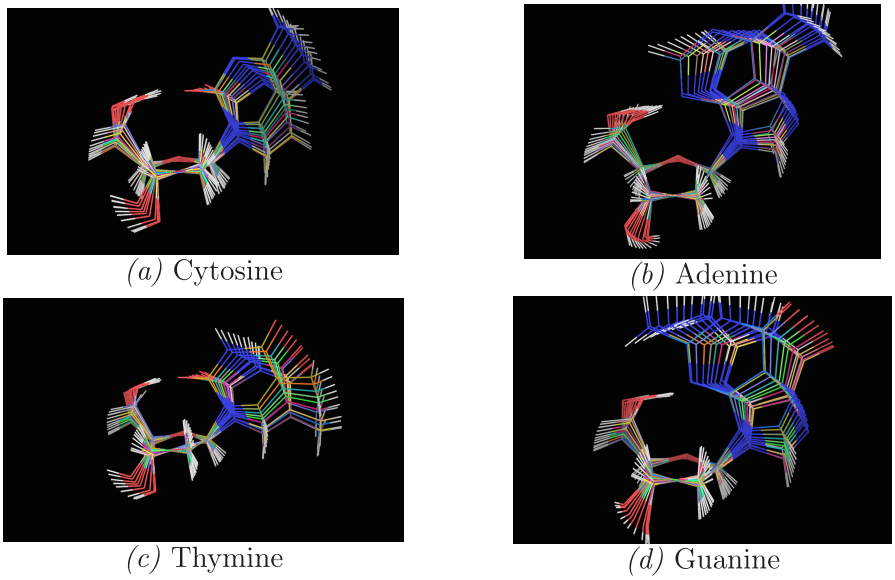

Figure 3. Illustration of the 20 representative path points for each of the four deoxyribonucleosides (a) **dC**, (b) **dA**, (c) **dT**, and (d) **dG** calculated by constrained optimizations using a fixed phase angle ϕ_2 and increments of 18°, e.g. ϕ_2 = 0, 18, 36, ..., 342°.

$$k_i^a = \mathbf{a}_i^\dagger \mathbf{K} \mathbf{a}_i \tag{15}$$

Local mode force constants, contrary to normal mode force constants, have the advantage of being independent of the choice of the coordinates used to describe the molecule in question and in contrast to vibrational frequencies they are independent of the atomic masses. They are extremely sensitive to differences in the electronic structure (e.g., caused by changing a substituent), and they capture only electronic effects directly associated with the intrinsic strength of the atom−atom interaction leading to a chemical bond as recently shown by Zou and Cremer.[49] Therefore, the local vibrational force constants provide a unique tool for assessing the strength of a chemical bond via vibrational spectroscopy, which has recently been applied to characterize strong and weak covalent bonds,[49−55] for the definition of new electronic parameters such as the generalized Tolman parameter[56−58] or a new aromaticity index.[48,59−61] In particular, weak chemical interactions including hydrogen, halogen, and pnicogen bonding were quantitatively assessed for the first time.[62−74]

In this work, we have used the local H-bond stretching frequencies ω^a and the local stretching force constants k^a for the characterization of the strength of the intramolecular H-bonds of the deoxyribonucleosides **dC**, **dA**, **dT**, and **dG**.

It is convenient to base the comparison of the bond strength of a series of molecules on a bond strength order (BSO) n rather than on a comparison for local force constant values. Both are connected via a power relationship according to the generalized Badger rule derived by Cremer and co-workers:[52,75]

$$\text{BSO } n = a(k^a)^b \tag{16}$$

The constants a and b in eq 16 can be determined via two reference values and the requirement that for a zero force constant the BSO n is zero. For H-bonds, n = 1 for the FH bond and n = 0.5 for the FH bond in the $[F\cdots H\cdots F]^-$ anion were used,[68] leading to a = 0.515 and b = 0.291, (calculated at the ωB97X-D/6-31++G(d,p) level of theory). According to eq 16 the OH bond in H_2O has a BSO n value of = 0.966. Therefore, we scaled the reference values, so that the BSO n of the OH bond in H_2O is 1.

QTAIM and NBO Analysis. Bader's quantum theory of atoms in molecules (QTAIM) presents the theoretical framework for identifying and characterizing chemical bonds and weak chemical interactions via the study of the topological features of the total electron density $\rho(r)$.[76,77] In this work we used QTAIM as a complementary tool to the local mode analysis to determine the covalent/electrostatic character of internal the H-bonds via the Cremer−Kraka criterion[78,79] of covalent bonding. According to this criterion a covalent bond between two atoms A and B is defined by the following two conditions: (i) *Necessary condition* The existence of a bond path and bond critical point $\mathbf{r}_c = c$ between A and B. (ii) *Sufficient condition* The energy density $H(\mathbf{r}_c) = H_c$ is smaller than zero. $H(\mathbf{r})$ is defined as

$$H(\mathbf{r}) = G(\mathbf{r}) + V(\mathbf{r}) \tag{17}$$

where $G(\mathbf{r})$ is the kinetic energy density and $V(\mathbf{r})$ is the potential energy density. The negative $V(\mathbf{r})$ corresponds to a stabilizing accumulation of density whereas the positive $G(\mathbf{r})$ corresponds to depletion of electron density.[79] As a result, the sign of H_c indicates which term is dominant.[80] If $H_c < 0$, the interaction is considered covalent in nature, whereas $H_c > 0$ is indicative of electrostatic interactions.

We complemented the QTAIM analysis with the natural bond orbital (NBO) of Weinhold and co-workers[81,82] in order to obtain further insights into the intermolecular orbital interactions, particularly the charge transfer from the nitrogen/oxygen lone pair to the adjacent σ^* of the O−H moiety stabilizing the H-bond. Within the NBO framework the delocalization energy ΔE_{del}(HB) associated with the electron delocalization between the nitrogen/oxygen lone pair (donor) and the σ^* of O−H moiety (acceptor) can be estimated via the charge transfer from the localized (donor) Lewis-type orbital (L) into the empty (acceptor) non-Lewis orbital (NL)[83,84]

$$E^2 = \Delta E_{del}(\text{HB}) = \frac{q_L F(\text{L, NL})^2}{\epsilon_{NL} - \epsilon_L} \tag{18}$$

where q_L is the orbital and ϵ_{NL} are the diagonal elements of the NBO Fock matrix corresponding to orbital energies of the donor orbital L and acceptor orbital NL, and F(L, NL) is the off-

DOI: 10.1021/acs.jpca.9b05452
J. Phys. Chem. A 2019, 123, 7087−7103

Table 1. Energies, Geometries, Vibrational, and Electron Density Data for Deoxyribonucleosides dA, dG, dC, and dT along Their Pseudolibration Paths[a]

ϕ_2 [deg]	q_2 [Å]	ΔE [kcal/mol]	ΔG [kcal/mol]	R(HB) [Å]	k^a(HB) [mdyn/Å]	ω^a(HB) [1/cm]	BSO n (HB)	ΔE_{del}(HB) [kcal/mol]	$\omega_\mu(\omega^a$, no., %) [1/cm]	ρ_c [e/ Å^3]	H_c [Hartree/ Å^3]	H_c/ρ_c [Hartree/e]
						dA						
270	0.256	−0.11(4.64)	−0.99(3.73)	1.866	0.226	638	0.372	20.4	130(5, 51.8)	0.232	−0.003	−0.011
288	0.304	−1.31(3.44)	−1.91(2.81)	1.909	0.152	524	0.353	18.7	130(5, 30.0), 114(4, 29.6)	0.211	−0.001	−0.006
306	0.272	−1.49(3.26)	−2.33(2.40)	1.969	0.138	499	0.330	15.4	112(4, 72.8)	0.185	−0.001	−0.005
324	0.214	−1.24(3.51)	−2.27(2.45)	1.971	0.144	510	0.329	15.6	106(4, 83.7)	0.184	−0.001	−0.004
342	0.173	−1.17(3.58)	−1.04(3.68)	1.951	0.156	531	0.337	17.2	100(4, 89.9)	0.192	−0.001	−0.004
0	0.165	−1.31(3.43)	−1.17(3.56)	1.941	0.151	523	0.341	18.2	97(4, 90.5)	0.197	−0.001	−0.004
18	0.186	−1.67(3.08)	−1.41(3.31)	1.948	0.159	536	0.338	18.2	99(4, 92.2)	0.194	−0.001	−0.003
36	0.234	−2.39(2.36)	−1.97(2.75)	1.959	0.164	544	0.333	17.9	100(4, 89.8)	0.190	−0.001	−0.004
54	0.291	−3.53(1.22)	−3.96(0.76)	1.945	0.135	493	0.339	19	98(4, 47.9), 76.3 (3, 27.9)	0.196	−0.001	−0.005
72	0.325	−4.52(0.15)	−4.64(0.09)	1.885	0.216	624	0.363	23.3	111(4, 38.7), 179(7, 28.5)	0.225	−0.002	−0.009
90	0.342	−4.68(0.07)	−4.77(−0.05)	1.826	0.249	670	0.390	28.3	182(7, 64.7)	0.258	−0.005	−0.021
108	0.343	−3.69(1.05)	−3.61(1.12)	1.784	0.326	767	0.409	32	194(7, 93.5)	0.285	−0.010	−0.034
126	0.326	−1.69(3.06)	−2.66(2.06)	1.799	0.163	543	0.411	31	6(1, 74.4)	0.288	−0.011	−0.037
						dG						
270	0.267	−0.76(3.76)	−1.40(3.49)	1.819	0.238	655	0.377	22.7	160(7, 45.6), 128(5, 23.8)	0.262	−0.007	−0.028
288	0.308	−2.22(2.31)	−2.80(2.09)	1.862	0.187	581	0.351	20.7	162(7, 38.1), 118(4, 27.0)	0.239	−0.005	−0.020
306	0.28	−2.45(2.08)	−3.53(1.36)	1.914	0.118	462	0.323	17.5	105(4, 46.0), 69 (3, 36.9)	0.212	−0.003	−0.014
324	0.23	−2.14(2.39)	−4.94(−0.04)	1.917	0.138	498	0.321	17.8	101(4, 54.4)	0.209	−0.002	−0.011
342	0.191	−1.96(2.57)	−1.73(3.17)	1.898	0.171	556	0.331	19.8	101(4, 83.0)	0.218	−0.002	−0.011
0	0.181	−2.00(2.53)	−1.80(3.09)	1.882	0.155	528	0.340	21.6	94(4, 78.1)	0.226	−0.003	−0.011
18	0.199	−2.28(2.24)	−1.90(3.00)	1.881	0.207	611	0.340	22.4	101(4, 85.4)	0.226	−0.002	−0.010
36	0.249	−2.95(1.58)	−2.56(2.34)	1.895	0.162	541	0.333	22	6(4, 65.7)	0.219	−0.002	−0.009
54	0.306	−3.98(0.55)	−4.09(0.81)	1.879	0.223	635	0.341	23.7	117(4, 47.2), 76 (3, 41.1)	0.228	−0.002	−0.011
72	0.336	−4.53(0.00)	−4.91(−0.01)	1.827	0.229	644	0.372	28.3	75(3, 50.6)	0.257	−0.005	−0.020
90	0.334	−3.78(0.74)	−3.99(0.91)	1.768	0.327	768	0.410	34.5	186(8, 48.3), 79 (3, 35.4)	0.296	−0.011	−0.039
108	0.304	−1.79(2.73)	−2.09(2.81)	1.732	0.38	828	0.436	38.4	194(8, 41.1), 199(9, 27.3)	0.323	−0.019	−0.057
						dC						
252	0.112	−0.17(2.95)	−1.73(1.36)	1.794	0.174	559	0.385	11.6	16(1, 56.9)	0.218	0.008	0.038
270	0.177	−0.85(2.27)	−1.71(1.38)	1.824	0.193	588	0.368	10	122(5, 65.6)	0.205	0.006	0.032
288	0.228	−1.61(1.51)	−1.96(1.13)	1.878	0.179	566	0.339	8	123(5, 73.3)	0.181	0.004	0.021
306	0.234	−1.85(1.27)	−2.38(0.70)	1.934	0.117	457	0.312	6.5	108(4, 83.4)	0.160	0.002	0.011
324	0.201	−1.51(1.61)	−2.21(0.88)	1.937	0.114	452	0.310	6.7	106(4, 93.4)	0.158	0.002	0.012
342	0.158	−1.12(2.00)	−1.10(1.99)	1.895	0.167	546	0.331	8.2	106(4, 73.2)	0.172	0.004	0.023
0	0.139	−0.91(2.21)	−0.63(2.46)	1.873	0.172	555	0.342	9.2	104(4, 79.0)	0.180	0.005	0.030
18	0.152	−0.87(2.26)	−0.63(2.46)	1.869	0.171	553	0.344	9.5	104(4, 82.1)	0.182	0.006	0.031
36	0.215	−1.15(1.98)	−0.79(2.30)	1.889	0.169	551	0.333	9	104(4, 89.9)	0.174	0.005	0.026
54	0.297	−2.13(0.99)	−2.47(0.62)	1.887	0.166	545	0.334	9.2	106(4, 84.6)	0.175	0.004	0.025
72	0.34	−3.06(0.07)	−3.08(0.01)	1.825	0.213	618	0.367	11.8	159(6, 40.6), 116(4, 33.9)	0.202	0.008	0.039
90	0.348	−2.72(0.40)	−2.64(0.45)	1.764	0.298	731	0.402	15.3	185(8, 50.5)	0.231	0.012	0.050
108	0.319	−0.88(2.24)	−1.35(1.74)	1.74	0.289	719	0.418	17.1	189(8, 91.1)	0.245	0.013	0.053
						dT						
270	0.19	−0.79 (3.10)	−1.44 (2.31)	1.868	0.277	576	0.348	8.7	111(5, 34.4), 191(9, 21.1)	0.214	0.009	0.043
288	0.25	−1.80(2.08)	−2.29(1.46)	1.933	0.113	451	0.321	7.1	110(5, 38.4), 94 (3, 34.5)	0.162	0.002	0.011
306	0.26	−2.24(1.65)	−2.67(1.08)	2.016	0.092	405	0.290	5.4	106(4, 88.1)	0.135	0.000	0.001
324	0.228	−1.96(1.93)	−2.62(1.13)	2.028	0.089	400	0.286	5.4	102(4, 89.8)	0.131	0.000	0.001
342	0.186	−1.58(2.31)	−1.05(2.69)	1.982	0.111	446	0.303	7	102(4, 92.9)	0.143	0.001	0.007
0	0.17	−1.41(2.47)	−1.05(2.69)	1.953	0.113	450	0.313	8.4	97(4, 92.3)	0.152	0.002	0.012
18	0.186	−1.48(2.41)	−0.93(2.81)	1.948	0.127	476	0.316	9.3	100(4, 95.5)	0.153	0.002	0.014
36	0.244	−1.96(1.93)	−1.74(2.01)	1.964	0.105	433	0.309	9.7	90(4, 94.5)	0.148	0.001	0.010
54	0.313	−3.05(0.84)	−3.04(0.71)	1.947	0.137	496	0.316	11.1	104(4, 93.0)	0.154	0.002	0.011

DOI: 10.1021/acs.jpca.9b05452
J. Phys. Chem. A 2019, 123, 7087−7103

Table 1. continued

ϕ_2 [deg]	q_2 [Å]	ΔE [kcal/mol]	ΔG [kcal/mol]	R(HB) [Å]	k^a(HB) [mdyn/Å]	ω^a(HB) [1/cm]	BSO n (HB)	ΔE_{del}(HB) [kcal/mol]	$\omega_\mu(\omega^a$, no., %) [1/cm]	ρ_c [e/ Å^3]	H_c [Hartree/ Å^3]	H_c/ρ_c [Hartree/e]
						dT						
72	0.35	−3.86(0.02)	−3.82(−0.08)	1.873	0.188	580	0.346	14.8	108(4, 44.4), 151(6, 23.0)	0.182	0.005	0.026
90	0.353	−3.30(0.58)	−3.17(0.58)	1.8	0.277	704	0.379	19.2	174(9, 93.1)	0.214	0.009	0.043
108	0.323	−1.24(2.65)	−1.49(2.26)	1.77	0.314	750	0.394	20.5	191(9, 93.2)	0.230	0.011	0.048

[a]Phase angles ϕ_2 are in degrees; puckering amplitudes q_2 are in angstroms; ΔE and ΔG indicate relative energy and Gibbs free energy in kilocalories per mole with respect to the planar form as reference, while the values in parentheses are relative to the global minimum as reference; bond length values R(HB) are in angstroms; force constants k^a are in millidyne per angstroms; vibrational frequencies ω^a(HB) are in inverse centimeters; ΔE_{del}(HB) gives the delocalization energy of lone-pair electrons from H-bond acceptor to H-bond donor in kilocalories per mole; $\omega_\mu(\omega^a$, no., %) represents the decomposition of H-bond normal modes to local stretching mode, ω^a is the vibrational frequency, no. is the name of normal mode given in number, and the contribution of normal mode to H-bond local stretching mode is given in percentage; electron densities ρ_c at the bond critical points are in electrons per cubic angstrom; energy densities H_c at the bond critical points are in Hartree per cubic angstrom; energy densities per electron H_c/ρ_c are in Hartree per electron. Calculated at the ωB97X-D/6-31++G(d,p) level of theory.

diagonal NBO Fock matrix element between the L and NL orbitals. The NBO analysis was applied to all conformers located on the pseudorotation paths to determine ΔE_{del}(HB) for all internal H-bonds.

Computational Methods. All calculations were performed with the ωB97X-D functional[85,86] and Pople's 6-31++G(d,p) basis set.[87−90] Tight convergence criteria were applied, (SCF iterations 10^{-10} Hartree and geometry optimizations 10^{-7} Hartree/Bohr) and an ultrafine grid was used for the DFT numerical integration.[91] First, the most stable conformer for each deoxyribonucleoside, e.g. the global minimum, was determined by fully optimizing the structures derived from all possible H-bond combinations using Cartesian coordinates. The pseudorotation path was then calculated in the following way. A puckering analysis was performed for the global minimum to obtain the corresponding phase angle ϕ_2 and the puckering amplitude q_2. Starting from this phase angle 20 representative path points were calculated by constrained optimizations with a fixed phase angle ϕ_2, modified in increments of 18° for e.g. ϕ_2 = 0, 18, 36, ..., 342°, as shown in Figure 3 to determine the pseudorotation path. For the constrained optimizations a mixed set of internal coordinates for the substituents and puckering coordinates for deoxyribose sugar ring was used.

Harmonic frequency calculations were carried out in each case to confirm the optimized conformers located on the pseudorotation path as minima (no imaginary frequency) or transition states (one imaginary frequency). In this regard, the pseudorotation path can be considered as a special reaction path with the phase angle ϕ_2 as reaction coordinate. For the lowest energy conformers being located on the opposite site of global minima, e.g. phase angles ϕ_2 in the range of ≈300°, a full geometry optimization was performed, to identify possible local minima, which were found for all deoxyribonucleosides in this range. For the highest energy conformers, e.g. phase angles ϕ_2 in the range of 330−18°, a full geometry optimization was performed to identify the transition state (TS) for the pseudorotation. The CESs were also mapped via constrained optimizations. For each fixed phase angle ϕ_2, the puckering amplitudes q_2 were constrained to four values, namely 0.1, 0.2, 0.3, and 0.4 Å, and the remainder of the molecule was optimized, leading to 80 data points for each CES. For each conformer on the pseudorotation path, a local mode analysis was performed for the investigation of the H-bond strength. Delocalization energies of the internal H-bonds were calculated for further characterization.[84] These energies reflect the delocalization of lone-pair electrons from H-bond accept or to H-bond donor

The RING Puckering program[26] was used for analysis of the deoxyribose sugar ring conformations. For the geometry optimizations and frequency calculations, a combination of the RING Puckering program and the program package Gaussian09[92] was used. All local mode analyses calculations were carried out with the program package COLOGNE2019.[93] The NBO calculations were carried out with NBO 6.[94] The QTAIM analysis was performed with the AIMALL software.[95]

RESULTS AND DISCUSSION

In Table 1, properties of the deoxyribonucleosides **dC**, **dA**, **dT**, and **dG** calculated at different phase angles ϕ_2 are listed. These comprise the puckering amplitude q_2, relative energy ΔE, and free energy ΔG with regard to the planar form and the global minimum, H-bond distance R(HB), force constant k^a(HB), local mode frequency ω^a(HB), and bond strength order BSO n(HB) as well the H-bond delocalization energy ΔE_{del}(HB) and the normal vibration mode(s) ω_μ with the highest H-bond contribution(s). Table 1 also contains the electron density ρ_c (e/Å^3) and the energy density H_c (Hartree/Å^3) at the bond critical point c. Table 2 summarizes H-bond properties of some

Table 2. Properties of Hydrogen Bonded Reference Complexes R1−R5[a]

molecule	k^a	BSO n	R(HB)	ρ_c	H_c	H_c/ρ_c
R1	0.209	0.360	1.905	0.183	−0.001	−0.005
R2	0.214	0.362	1.895	0.176	0.002	0.012
R3	0.044	0.241	2.457	0.071	0.003	0.048
R4	0.116	0.309	1.981	0.162	−0.004	−0.027
R5	0.205	0.358	1.922	0.202	0.000	0.002

[a]Force constants k^a are in millidyne per angstrom; H-bond lengths R(HB) are in angstroms, ρ_c values are in electrons per cubic angstrom; H_c values are in Hartree per cubic angstrom; energy densities per electron H_c/ρ_c are in Hartree per electron. Reference complexes **R1−R5** are shown in Figure 9. Calculated at the ωB97X-D/6-31++G(d,p) level of theory.

reference molecules. In Table 3, geometric features, including R(HB), angles α_1 and α_2, and dihedral angles τ_1 and τ_2 between the base and the CH_2OH group forming the intramolecular H-bond of the conformer with the strongest H-bond (ϕ_2 = 108°), and that with the weakest H-bond (ϕ_2 = 324°) are summarized for puckering amplitude values of 0.1, 0.2, 0.3, and 0.4 Å.

CESs and Pseudorotation (Pseudolibration) Paths. The pseudorotation paths on the corresponding CESs of the

DOI: 10.1021/acs.jpca.9b05452
J. Phys. Chem. A 2019, 123, 7087−7103

Table 3. Geometric Features of Conformers at $\phi_2 = 108°$ (Region of Strongest H-Bonds) and $\phi_2 = 324°$ (Region of Weakest H-Bonds)[a]

	q_2 [Å]	r(HB) [Å]	α_1 [deg]	α_2 [deg]	τ_1 [deg]	τ_2 [deg]	$\sum(\alpha_1, \alpha_2)$ [deg]	$\Delta(\tau_1, \tau_2)$ [deg]	ΔE [kcal/mol]
					dA				
$\phi_2 = 108°$	0.1	1.800	23.9	32.2	54.8	−93.5	56.1	38.6	−0.76
	0.2	1.784	21.9	36.4	55.7	−93.4	58.4	37.7	−2.25
	0.3	1.783	20.3	40.0	56.8	−93.4	60.3	36.7	−3.52
	0.4	1.787	18.7	42.9	57.0	−92.2	61.6	35.2	−3.34
$\phi_2 = 324°$	0.1	1.872	25.7	23.7	51.3	−89.1	49.4	37.8	−0.74
	0.2	1.929	25.4	20.0	49.0	−86.5	45.4	37.5	−1.22
	0.3	1.988	24.9	16.8	47.6	−85.3	41.8	37.7	−0.78
	0.4	2.073	23.4	13.6	56.4	−85.6	36.9	29.2	1.21
					dG				
$\phi_2 = 108°$	0.1	1.747	23.2	30.9	64.3	−81.7	54.2	17.4	−0.23
	0.2	1.732	21.4	35.4	64.6	−83.0	56.7	18.4	−1.15
	0.3	1.732	19.7	39.2	65.2	−83.2	58.9	18.0	−1.79
	0.4	1.735	18.0	42.3	65.4	−82.0	60.3	16.6	−0.85
$\phi_2 = 324°$	0.1	1.825	25.1	21.9	60.8	−77.1	47.0	16.3	−1.29
	0.2	1.893	24.7	18.0	57.9	−75.7	42.7	17.8	−2.09
	0.3	2.000	24.3	14.3	55.4	−76.0	38.6	20.6	−1.72
	0.4	2.201	23.6	10.8	54.4	−77.9	34.3	23.5	0.50
					dC				
$\phi_2 = 108°$	0.1	1.759	23.6	30.9	63.6	−97.7	54.5	34.1	0.34
	0.2	1.742	21.1	35.2	64.8	−97.9	56.4	33.1	−0.19
	0.3	1.738	19.1	39.1	64.7	−97.8	58.2	33.1	−0.85
	0.4	1.750	17.3	42.3	63.4	−97.1	59.5	33.6	−0.25
$\phi_2 = 324°$	0.1	1.837	25.5	22.9	59.9	−91.1	48.4	31.2	−1.04
	0.2	1.937	24.8	19.5	58.6	−87.8	44.3	29.2	−1.51
	0.3	2.128	23.8	16.4	58.2	−86.7	40.2	28.6	−0.91
	0.4	2.672	22.1	12.9	62.7	−88.5	35.0	25.8	0.90
					dT				
$\phi_2 = 108°$	0.1	1.789	23.6	31.4	60.8	−98.3	55.0	37.5	0.20
	0.2	1.773	21.2	35.6	62.1	−98.6	56.7	36.5	−0.45
	0.3	1.768	19.2	39.3	61.5	−98.9	58.5	37.4	−1.20
	0.4	1.779	17.5	42.4	60.3	−98.5	59.8	38.2	−0.65
$\phi_2 = 324°$	0.1	1.878	25.5	23.5	56.6	−92.2	49.1	35.6	−1.20
	0.2	1.986	24.9	20.2	54.7	−89.2	45.1	34.5	−1.91
	0.3	2.198	24.1	17.3	54.5	−88.0	41.3	33.5	−1.65
	0.4	2.811	22.4	14.1	59.6	−89.7	36.5	30.1	−0.30

[a] $\phi_2 = 108°$ corresponds to the envelope form E_4, and $\phi_2 = 324°$ corresponds to the envelope form E_5; see Figure 2. $\sum(\alpha_1, \alpha_2)$ is the sum of angles α_1 and α_2. $\Delta(\tau_1, \tau_2)$ is the difference of $|\tau_2| - \tau_1$. ΔE is the conformational energy with regard to the planar form. Calculated at the ωB97X-D/6-31++G(d,p) level of theory.

deoxyribonucleosides **dC**, **dA**, **dT**, and **dG** are shown in Figure 4. We found on the pseudorotation paths of all deoxyribonucleosides negative puckering amplitudes in the range of $\phi_2 = 108$ to 270° indicating a ring inversion. As an example, the ring inversion for **dT** is shown in Figure 5 for conformer 1 (green color) with $\phi_2 = 108°$ and $q_2 = +0.323$ Å and conformer 2 (red color) with $\phi_2 = 144°$ and $q_2 = -0.228$ Å. This inversion leads to an incomplete pseudorotation, i.e. the pseudorotation path is not a closed circle as expected (see Figure 2) but an open curve, which we coined as pseudolibration path. As discussed in the Supporting Information for **dA** as an example, the energies beyond the ring inversion point are higher than the energy of the planar form, and as such there is no longer a minimum energy path on the CES. This suggests that when the deoxyribonucleoside reaches the end-point of the path (e.g., ring inversion point) during a thermal motion, it prefers to return back to the energetically lower part of CES via the pseudolibration path instead of entering the high energy regions.

On each of the pseudolibration paths a global minimum in the range of $\phi_2 = 72-90°$ and a local minimum in the range of $\phi_2 = 306°$ separated by a transition state in the range of $\phi_2 = 18-342°$ was identified, as shown in Figure 4. Energy differences ΔE between the global and local minima are 3.24, 2.05, 1.26, and 1.65 kcal/mol, respectively for **dA**, **dG**, **dC** and **dT**; see also Table 1. The puric bases (**dA** and **dG**) process somewhat larger ΔE values compared to the pyrimidic bases (**dC** and **dT**) which is also reflected by the fact that the former possess longer pseudolibration paths, i.e., they are conformationally more flexible. The transition states for the pseudolibration are located at $\phi_2 = 337.7°$, 347.5°, 13.5°, and 4.7° for **dA**, **dG**, **dC**, and **dT**. The corresponding pseudolibration barriers from the global minimum to the local minimum are 3.59, 2.58, 2.26, and 2.48 kcal/mol for **dA**, **dG**, **dC**, and **dT**. The reverse barriers, e.g. from local minimum to global minimum, are only 0.34, 0.53, 1, and 0.84 kcal/mol; see Table 1.

DOI: 10.1021/acs.jpca.9b05452
J. Phys. Chem. A 2019, 123, 7087−7103

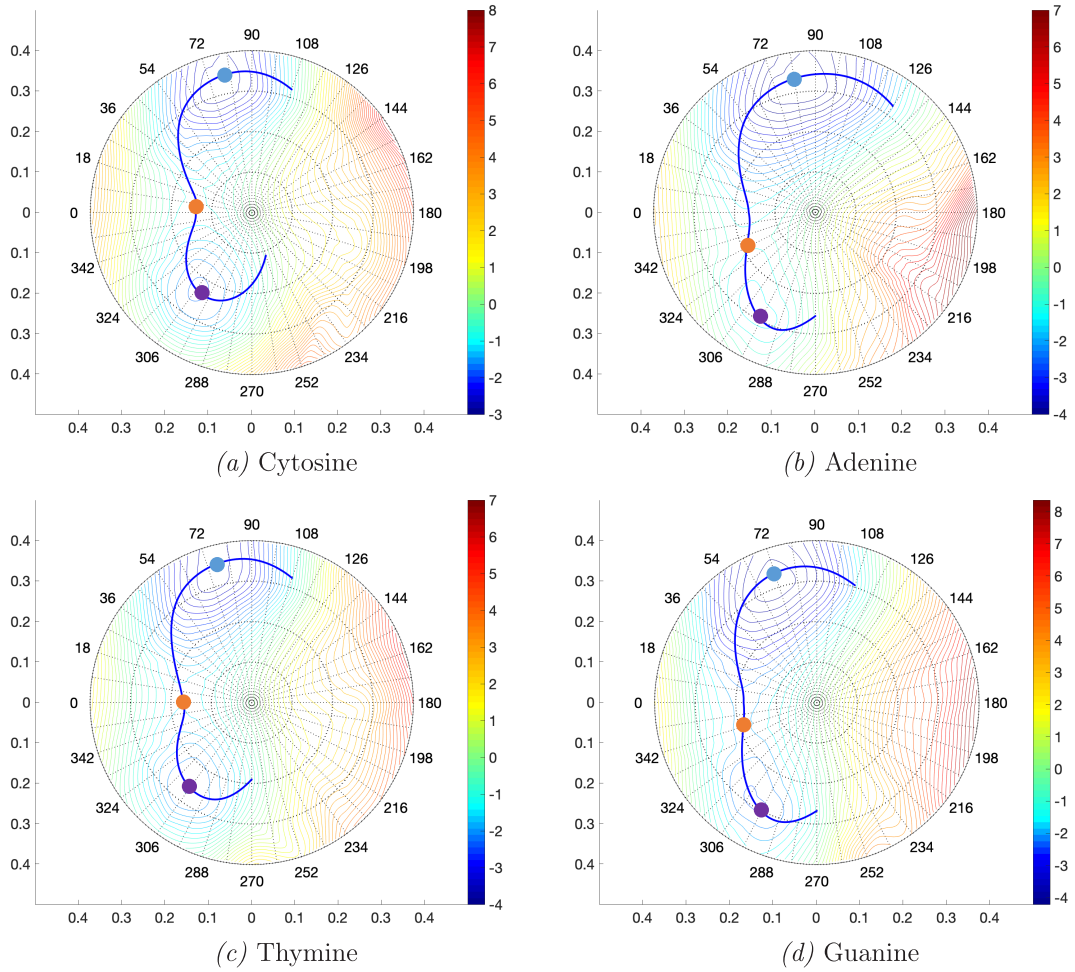

Figure 4. Conformational energy surfaces (CESs) and pseudolibration paths of deoxyribonucleosides **dC** (a); **dA** (b); **dT** (c); and **dG** (d). At the center of each CES, the planar deoxyribose ring form is located. The corresponding energy is used as reference. Both *x* and *y* axes show the magnitude of puckering amplitude q_2 in angstroms. The outer radius of the CES represents the maximum puckering amplitude of 0.4 Å. The labels around the CES circle denote the value of the phase angle ϕ_2 in degrees. The solid blue line indicates the pseudolibration path. The color bar represents the energy on the CES in kilocalories per mole relative to the planar form: (*yellow to red regions*) location of conformers higher in energy than the planar form; (*green to blue regions*) location of conformers lower in energy than the planar form. The blue dot in the range 72−90° shows the location of the global, the purple dot near 306° shows the location of the local minimum, and the yellow dot in the range 18−342° shows the transition state between the two forms. Calculated at the ωB97X-D/6-31++G(d,p) level of theory.

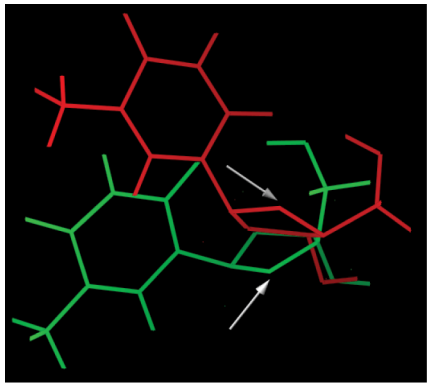

Figure 5. Ring inversion of the sugar ring (marked by silver arrows) of **dT**; conformer 1 is shown in green, ϕ_2 = 108° and q_2 = +0.323 Å, and conformer 2 is shown in red, ϕ_2 = 144° and q_2 = −0.228 Å.

More detailed information is obtained by plotting changes of ΔE, q_2, R(HB), and BSO n(HB) as a function of ϕ_2 as shown in Figure 6. The pseudolibration paths can be divided into three distinct regions; (1) *Global minimum region*: including all conformers *n* with an energy difference $\Delta E = (E_n - E_{global})$ less than 1.0 kcal/mol. For all deoxyribonucleosides, this region covers ϕ_2 angles in the range of 54−90°. (2) *Local minimum region*: including all conformers *m* with an energy difference $\Delta E = (E_m - E_{local})$ less than 0.5 kcal/mol. For all deoxyribonucleosides, this region covers ϕ_2 angles in the range of 288−324°. (3) *Transition region*: Including all conformers in between, e.g. ϕ_2 angles in the range of 342−36°; see Figure 6. All conformers located either in the global or minimum region were identified to have no imaginary frequencies. All other conformers in the transition region and the regions outside the global and local minima (ϕ_2 angles in the range of 234−270° and 108−144°) were identified to have one imaginary frequency.

A comparison of Figure 6a and b reveals how the puckering amplitude and the conformational energy are related. All deoxyribonuclesides feature the same deoxyribose ring puckering pattern: the strongest puckering occurs in the global minimum region (ϕ_2 = 72−90°, q_2 values up to 0.35 Å), followed by the puckering in the local minimum region (ϕ_2 =

DOI: 10.1021/acs.jpca.9b05452
J. Phys. Chem. A 2019, 123, 7087−7103

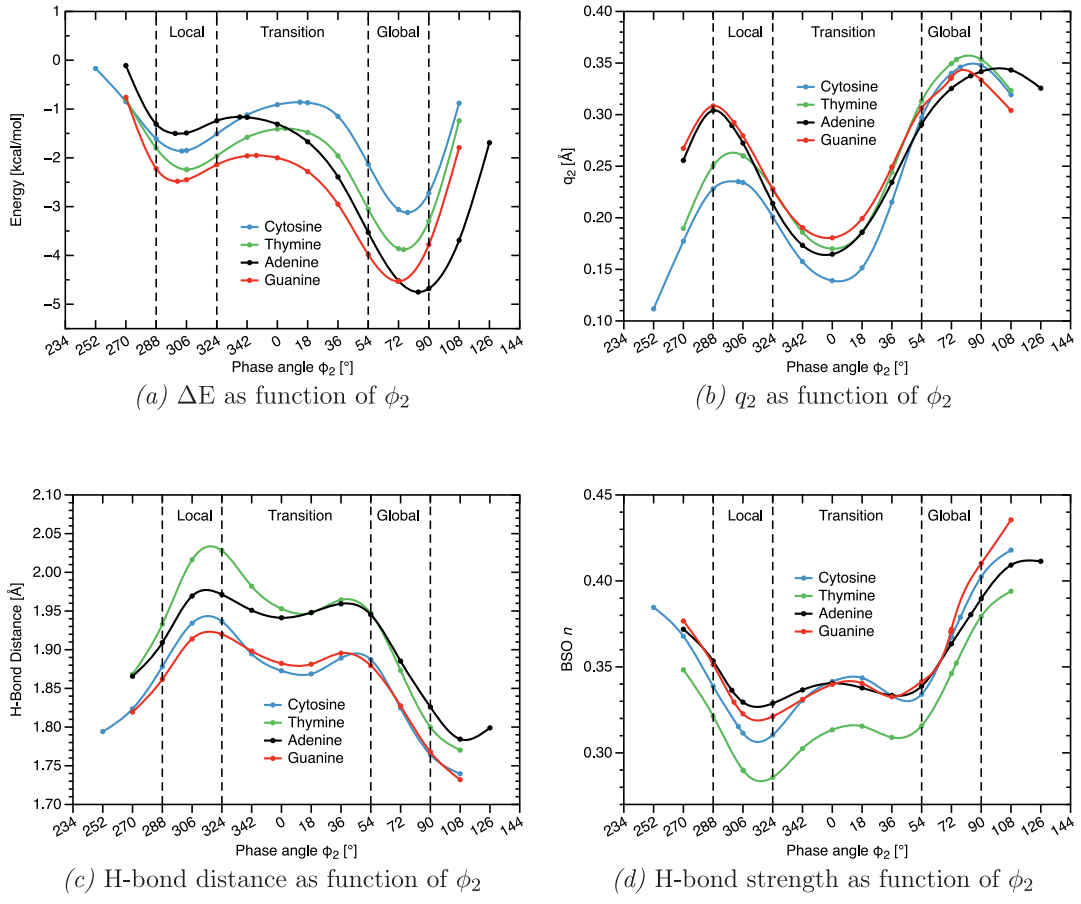

(a) ΔE as function of ϕ_2 (b) q_2 as function of ϕ_2

(c) H-bond distance as function of ϕ_2 (d) H-bond strength as function of ϕ_2

Figure 6. (a) Changes of the conformational energy ΔE with regard to the planar form, (b) puckering amplitude q_2, (c) H-bond distance R(HB), and (d) H-bond strength order BSO n along the pseudolibration path described as a function of the puckering angle ϕ_2. The local minimum, transition, and global minimum regions are denoted by vertical dashed lines. For a definition of these regions, see the text. Calculated at the ωB97X-D/6-31++G(d,p) level of theory.

288−306°, q_2 values up to 0.31 Å), while the smallest puckering (q_2 = 0.15−0.18 Å) occurs in the transition region in the range of ϕ_2 = 324−54°, suggesting that the larger the puckering amplitude, the lower the conformational energy. This holds for the pyrimidic bases **dC** and **dT** for which the energy and amplitude curves are perfect mirror images, e.g. smallest amplitude values correspond to highest energy values. The puckering amplitude curves of the puric bases **dA** and **dG** are almost identical in the local energy region, whereas the difference in the conformational energy is up to 1 kcal/mol. This shows that there are additional factors determining the conformational energy, such as constrained flexibility via H-bonding which in turn can be different for the different bases.

Figure 6c and d shows the change of the internal H-bond distance R(HB) and the corresponding H-bond strength BSO n along the pseudolibration path. There is a direct relationship between H-bond length and strength, i.e. the strongest H-bonds are the shortest as also reflected by Figure 7. This is not always true as numerous examples have shown.[96,97] Figure 7 reveals that there is a considerable variation in the H-bond lengths (0.334 Å) leading to H-bond strength differences of 0.15.

There is no obvious correlation between the H-bond length/strength and the conformational energy change. The longest and weakest H-bonds are found in the local minimum region for all deoxyribonuclesides, with the longest H-bond of 2.028 Å at ϕ_2 = 324° for **dT** compared with 1.917 Å at ϕ_2 = 324° for **dG**. If the H-bond strength would dominate the conformational energy,

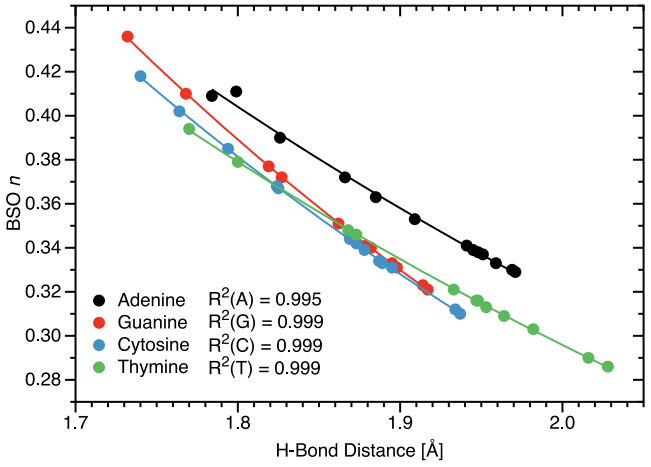

Figure 7. Correlation between H-bond strength and H-bond length. Calculated at the ωB97X-D/6-31++G(d,p) level of theory.

according to Figure 6a the longest H-bonds should be located in the transition region and at the end points of the pseudolibration paths. However, we find for all deoxyribonucleosides smallest BSO n values at the end of local minimum region (ϕ_2 = 306−324°) which increase through the transition region to the global minimum region (ϕ_2 = 54−90°). However, the shortest and strongest H-bonds are located outside both the global minimum region (1.732 Å at ϕ_2 = 108° for **dG**) and the local minimum

DOI: 10.1021/acs.jpca.9b05452
J. Phys. Chem. A 2019, 123, 7087−7103

region (1.794 Å at $\phi_2 = 252°$ for **dC**), i.e. at the turning points of the pseudolibration path, where the deoxyribonuclesides bounce back into the opposite path direction. These results clearly reveal that H-bonding determines the shape and length of the pseudolibration paths.

Internal H-Bond Strength and Covalent/Electrostatic Character. The weakest H-bond (BSO $n = 0.286$) is found for the **dT** conformer at $\phi_2 = 324.0°$ which is still stronger than the H-bond in the formaldehyde dimer **R3**, (BSO $n = 0.241$, see Table 2). The **dG** conformer at $\phi_2 = 108.0°$ has the strongest H-bond (BSO $n = 0.436$)—see Figure 8—which is even stronger

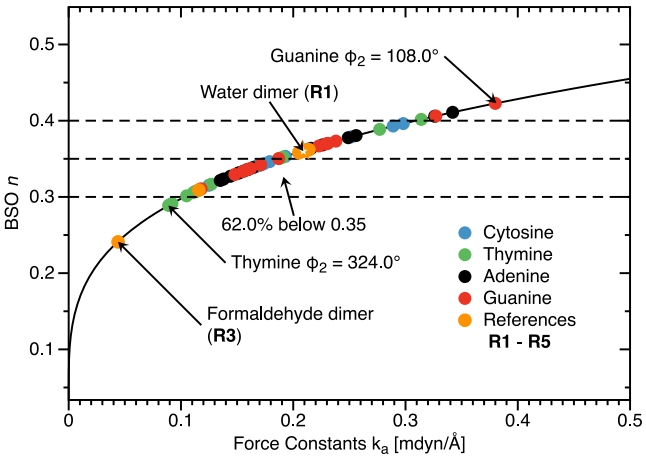

Figure 8. Bond strength BSO n of the H-bonds of all deoxyribonucleoside conformers as a function of the corresponding local stretching force constant k^a as determined via eq 16. For comparison H-bonded complexes **R1**−**R5** defined in Figure 9 are included. Dashed horizontal lines mark BSO n values of 0.3, 0.35, and 0.4, respectively. Calculated at the ωB97X-D/6-31++G(d,p) level of theory.

than the H-bond in the water dimer R1 with a BSO n value of 0.360; see Table 2. The percentage of conformers with BSO n values between 0.3 and 0.35 is 62.0%, in the range of the most common H-bond types in water clusters.[68] This clearly shows that the intermolecular H-bonds are of considerable strength and that they are an important feature of deoxyribonucleosides.

In addition to the H-bond strength we evaluated the covalent/electrostatic character of the H-bonds applying the Cremer−Kraka criterion of covalent bonding[78−80,98] described above. As reflected by data in Table 1 H_c/ρ_c values range from −0.057 Hartree/e (covalent character) for **dG** at the $\phi_2 = 108°$ turning point (strongest H-bond, BSO $n = 0.436$) to 0.053 Hartree/e (electrostatic character) for **dC** again at the $\phi_2 = 108°$ turning point (second strongest H-bond, BSO $n = 0.418$). Similar values were also found for the H-bonds of the reference compounds **R1**−**R5** shown in Figure 9 as revealed by the data in Table 2. These H_c/ρ_c magnitudes are typical of H-bonding[99] and small compared with the corresponding values for the OH bond in H_2O (−1.666 Hartree/e) and the H-donor bond in **R1** (−1.689 Hartree/e).[68,100,101]

In Figure 10a normalized energy density H_c/ρ_c values are correlated with the amplitudes q_2 for all conformers of the four deoxyribonucleosides. As expected there is no general relationship because the amplitude q_2 is a more global property reflecting complex geometry changes induced by ring puckering while H_c/ρ_c is taken only at a single point. However, one finds a clear separation into puric and pyrimidic bases caused by the different sign of the corresponding H_c/ρ_c values. In Figure 10b,

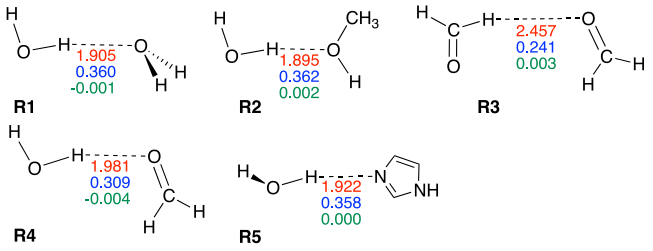

Figure 9. Reference complexes **R1**−**R5**. The intramolecular H-bond distance (Å) is given in red, the corresponding BSO n value is in blue, and energy density H_c (Hartree/Å^3) is in green. Calculated at the ωB97X-D/6-31++G(d,p) level of theory.

BSO n values are correlated with H_c/ρ_c. There is no overall relationship between BSO n and H_c/ρ_c for all conformers. However, there is a correlation between BSO n and H_c/ρ_c for the puric bases **dA** and **dG** as well as for the pyrimidic bases **dC** and **dT**. Larger BSO n values correspond to larger H_c/ρ_c magnitudes in both cases.

The finding that **dA** and **dG** conformers possess negative H_c/ρ_c values, i.e. being located on the covalent side of Figure 10, whereas all **dC** and **dT** conformers possess positive H_c/ρ_c, i.e. being located on the electrostatic side of Figure 10, which reflects the influence of the base determining (i) the different H-bond type, [O−H···N] for the puric bases and [O−H···O] bonds for the pyrimidic bases, and (ii) leading to a different electronic environment, i.e. in the more bulky puric bases the electron density can delocalize more than in the pyrimidic bases influencing the lone pair density of the H-bond acceptor atom. This will be discussed in more detail in the following.

Influence of the Orientation of the CH_2OH Group and the Base on H-Bonding. As discussed above (see Figure 7) there is a correlation between H-bond distance and H-bond strength for all four deoxyribonucleosides, but no obvious correlation between the conformational energy and H-bond distance, in particular in the local and transition region, (see Figure 6a and c), which needs further analysis. The H-bond distance depends on the mutual orientation of the CH_2OH substituent (*H-bond donor*) of the C5 sugar ring carbon and the base (*H-bond acceptor*) attached to the C2 sugar ring carbon, which in turn depends on the ring pucker. This mutual orientation is also critical for optimal orbital overlap, i.e. the O−H should point to the lone pair of the H-bond acceptor atom A (A = N for **dA**, **dG**; A = O for **dC**, **dT**) in a way that the angle (OHA) is close to 180°.[101]

For the quantification of this orientation we used two torsion angles, defined in Figure 11; torsion angle τ_1 describing the rotation of the base and torsion angle τ_2 describing the rotation of the CH_2OH group perpendicular to the sugar ring. The dihedral difference $\Delta(\tau_1, \tau_2) = |\tau_2| - \tau_1$ can serve as measure of the distance between H-bond donor and acceptor; i.e. smaller dihedral differences indicate shorter H-bonds and in this way stronger H-bonds. For the global minimum geometries the dihedral differences $\Delta(\tau_1, \tau_2)$ are 24.3°, 1.3°, 13.1°, and 16.3° for **dA**, **dG**, **dC**, and **dT**, respectively. For the local minimum geometries $\Delta(\tau_1, \tau_2)$ are larger with values of 43.1°, 25.1°, 33.8°, and 39.1° for **dA**, **dG**, **dC**, and **dT**, respectively. This reveals that for the global minimum geometries H-bond interactions are stronger. The largest difference between the global and the local minimum $\Delta(\tau_1, \tau_2)$ values are found for **dG** (23.8°), followed by **dT** (22.8°), **dC** (20.7°), and **dA** (18.8°). Obviously, in the local minimum region, i.e. for puckering angles ϕ_2 between 288° and

DOI: 10.1021/acs.jpca.9b05452
J. Phys. Chem. A 2019, 123, 7087−7103

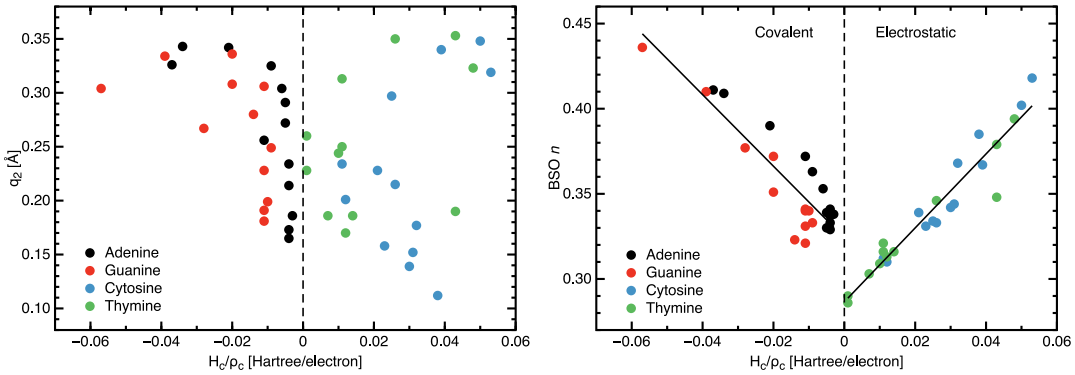

(a) Amplitude q_2 and H_c/ρ_c (b) BSO n and H_c/ρ_c

Figure 10. (a) Correlation between amplitude q_2 and normalized energy density H_c/ρ_c. (b) Correlation of BSO n and normalized energy density H_c/ρ_c. Calculated at the ωB97X-D/6-31++G(d,p) level of theory.

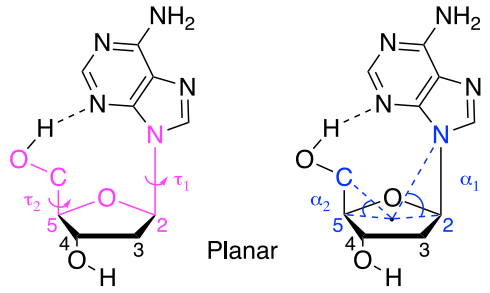

Figure 11. Definition of torsion angles τ_1 and τ_2 (pink color) and angles α_1 and α_2 (blue color) as listed in Table 3.

324° the CH_2OH group and the base cannot orient in an optimal way.

Besides a rotational movement the substituents can tilt relative to the main plane of the deoxyribose ring described by angles α_1 and α_2 for the base and the CH_2OH group respectively, as shown in Figure 11. For the global minimum geometries the tilting angle α_2 of the CH_2OH adapts values of 37.1°, 34.1°, 35.6°, 35.3° for **dA**, **dG**, **dC**, and **dT**, respectively. For the local minimum geometries α_2 values are smaller: 17.3°, 14.6°, 18.3°, and 18.3° for **dA**, **dG**, **dC**, and **dT**, respectively. The tilting angles α_1 of the base are 15.2°, 13.3°, 12.4°, and 12.1° for the global minimum geometries and 29.0°, 29.1°, 28.0°, and 27.8° for the local minimum geometries of **dA**, **dG**, **dC**, and **dT**, respectively. The sum $\sum(\alpha_1, \alpha_2)$ of the tilting angles α_1 and α_2 reflects the distance between H-bond donor and acceptor. The larger the sum $\sum(\alpha_1, \alpha_2)$, the smaller the distance between the H-bond donor and acceptor and the stronger is the H-bond. For the puric bases, the differences of $\sum(\alpha_1, \alpha_2)$ between the global and local minimum geometries are 6.1° and 3.6° for **dA** and **dG**, respectively. The corresponding differences for the pyrimidic bases are somewhat smaller with 1.7° and 1.4° for **dC** and **dT**, respectively. This indicates that the tilting movement is more pronounced for the puric bases although they are more bulky than their pyrimidic counterparts. Overall, our analysis suggests that side group rotation is more important for the H-bond formation than tilting.

The strength of the H-bond also depends on the orientation and electron density distribution of the lone pair of the H-bond acceptor atom (N, respectively O). Both can be assessed via the delocalization energy ΔE_{del}(HB) as defined in eq 18. The larger ΔE_{del}(HB), the stronger the H-bond.[83,84] As revealed by the data in Table 1 larger ΔE_{del} values along the pseudolibration paths are found for the puric bases **dA** and **dG** than for the pyrimidic bases **dC** and **dT**. ΔE_{del} values for the pyrimidic bases at the global minima are 32.0 kcal/mol (ϕ_2 = 108°, q_2 = 0.343 Å) for **dA** and 38.4 kcal/mol (ϕ_2 = 108°, q_2 = 0.304 Å) for **dG**, compared to the pyrimidic bases, 17.1 kcal/mol (ϕ_2 = 108°, q_2 = 0.319 Å) for **dC** and 20.5 kcal/mol (ϕ_2 = 108°, q_2 = 0.323 Å) for **dT**. This is in line with the finding that puric bases generally tend to have a more delocalized electron density than pyrimidic bases[102] inducing a more delocalized electron density at the lone pair of the H-bond acceptor atom and in this way leading to stronger H-bonding. This is in line with our finding that H-bonding in the puric bases is of more covalent nature and that the global minimum conformation of **dG** has the strongest H-bond of all conformers investigated in this work with a BSO n value of 0.436.

In order to gain additional insights into these important side group effects and for better comparison, we evaluated torsion and tilting angles for all deoxyribonucleosides for the same two puckering modes, ϕ_2 = 108° and ϕ_2 = 324° (envelope forms E_4 and E_5, respectively, see Figure 2), corresponding to strong and weak H-bond regions and for four different amplitudes 0.1, 0.2, 0.3, and 0.4 Å mapping the angle changes along the CES; see Table 3. As suggested by the pseudorotational cycle shown in Figure 2, ring puckering for the ϕ_2 = 108° conformation should allow a better interaction between the CH_2OH group and the base than that for ϕ_2 = 324°.

According to the data in Table 3 for puckering mode E_4, α_1 is decreasing whereas α_2 is increasing for increasing puckering amplitudes for all deoxynucleosides. These two opposite movements balance each other, so that as a consequence, the $\sum(\alpha_1, \alpha_2)$ is increasing to 61.6°, 60.3°, 59.5°, and 59.8° for **dA**, **dG**, **dC**, and **dT**, respectively, reflecting strong H-bonding. It is also noteworthy, that the effect is almost similar for all deoxyribonuclesides quantifying the trends shown in Figure 6. In contrast, for puckering mode E_5 both α_1 and α_2 are decreasing for increasing amplitudes, so that the $\sum(\alpha_1, \alpha_2)$ is also decreasing to 36.9°, 34.3°, 35°, and 36.5° for **dA**, **dG**, **dC**, and **dT**, respectively, reflecting weak H-bonding. In addition, the decreasing values of both tilting angles indicate that the equatorial position is more favorable when the ring puckers with a larger amplitude. As shown in Table 3 overall changes in $\Delta(\tau_1, \tau_2)$ for increasing puckering amplitudes are somewhat less pronounced. Overall this analysis shows that both the puckering amplitude and the puckering mode have a substantial influence on H-bond formation.

DOI: 10.1021/acs.jpca.9b05452
J. Phys. Chem. A 2019, 123, 7087−7103

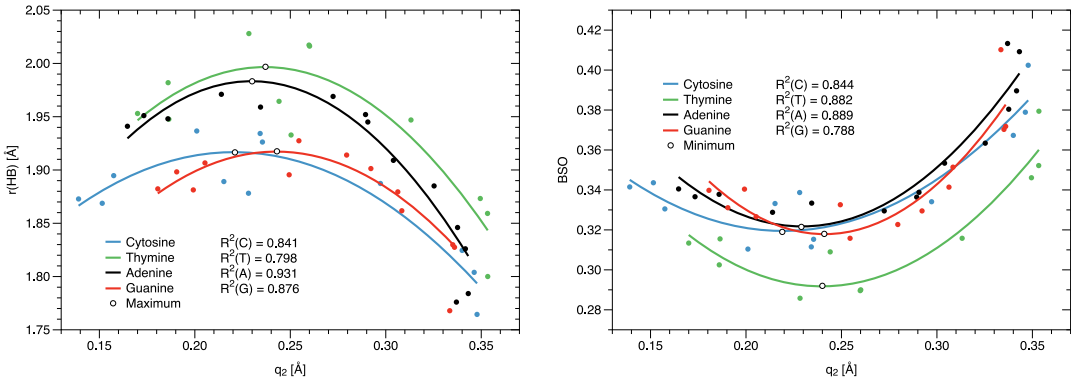

(a) Amplitude q_2 and H-bond distance (b) Amplitude q_2 and H-bond strength

Figure 12. (a) Correlation of puckering amplitude q_2 and H-bond distance, (b) correlation of puckering amplitude q_2 and H-bond strength, expressed as a quadratic function of the puckering amplitude q_2. The color points indicate the original calculated data. The lines represent the corresponding H-bond property as a quadratic function of q_2. The curve maxima (a) and minima (b) are denoted by open cirles. Calculated at the ωB97X-D/6-31++G(d,p) level of theory.

Interplay of Ring Puckering and Internal H-Bonding. In the following it will be discussed how the puckering amplitude q_2 is related to the H-bond length/strength. As shown in Figure 12, there is a qualitative quadratic relationship between the two quantities.

An increase of the puckering amplitude q_2 first leads to an increase of the H-bond length (Figure 12a) reaching a maximum value around q_2 = 0.25 Å, followed by a decrease of the H-bond length for larger puckering amplitudes. This corresponds to a decrease of the H-bond strength, reaching a minimum value around 0.25 Å, followed by an increase of the bond strength (Figure 12b). This is in line with Figure 6c revealing that at the local minima on the CESs located around the puckering angle ϕ_2 = 306° with puckering amplitudes q_2 in the range of 0.23 and 0.27 Å (see Figure 6b) the longest H-bonds are found. After passing through the local minima, the H-bond distances decrease until reaching minimum values beyond the global minima at the turning points of the pseudolibration paths. This implies that the H-bond strength increases along the pseudolibration path from the local minimum, through the transition state, to the global minimum on CES and beyond as a result of ring puckering, clarifying that there is no direct relationship between the conformational energy and the H-bond length/strength, which would have implied longest/weakest H-bonds in the transition region.

Comparison with H-Bond Free Model Analogues. Finally we studied the four H-bond free deoxyribonucleosides analogs **dmC**, **dmA**, **dmT**, and **dmG** shown in Figure 13 in order to determine (i) if the pseudolibration path on the CES surface converts into a full pseudorotation path if the H-bonding is eliminated and (ii) if there is still a global and local minimum separated by a transition state.

The CESs of the H-bond free analogs are shown in Figure 14. For all analogs there exists still a pseudolibration path, which for the pyrimidic bases **dCm** and **dTm** is considerably longer compared with their original counterparts. That means that removal of the H-bond does not restore the full conformational flexibility of the sugar ring. We still find global and local minima separated a transition state on the CESs of **dCm** and **dTm** (see Figure 14a and c). However, without the influence of the internal H-bond, the transition region shrinks from ϕ_2 = 342°−36° to ϕ_2 = 342°−18° and the position of local and global minima are exchanged. In the case of the puric bases **dAm** and

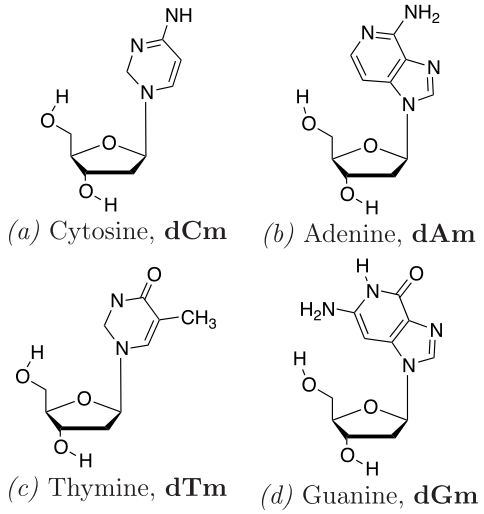

(a) Cytosine, **dCm** (b) Adenine, **dAm** (c) Thymine, **dTm** (d) Guanine, **dGm**

Figure 13. H-bond free deoxyribonucleoside analogs **dCm**, **dAm**, **dTm**, and **dGm**.

dGm only one minimum is found at ϕ_2 = 342° and the pseudolibration paths do not become considerably longer. This suggests that H-bonding invokes more strain on the pyrimidic bases, which is line with the above finding that pyrimidic H-bonding is more covalent in nature.

CONCLUSIONS AND OUTLOOK

In this study, the Cremer−Pople ring puckering analysis and the Konkoli−Cremer local mode analysis supported by the topological analysis of the electron density were applied to systematically analyze for the first time the interplay between deoxyribose ring puckering and the intramolecular H-bonding in 2′-deoxycytidine (cytosine), **dC**, 2′-deoxyadenosine (adenine), **dA**, thymidine (thymine), **dT**, and 2′-deoxyguanosine (guanine), **dG**. Using Cremer−Pople puckering coordinates, the CES for any substituted ring system such as a deoxyribonucleoside can be determined in analytical form and a physically meaningful pseudorotation path is obtained. Local mode force constants are a unique measure of bond strength. Our work has led to the following conclusions:

1. We found for all four deoxyribonucleosides **dC**, **dA**, **dT**, and **dG** incomplete pseudorotation paths on the CESs

DOI: 10.1021/acs.jpca.9b05452
J. Phys. Chem. A 2019, 123, 7087−7103

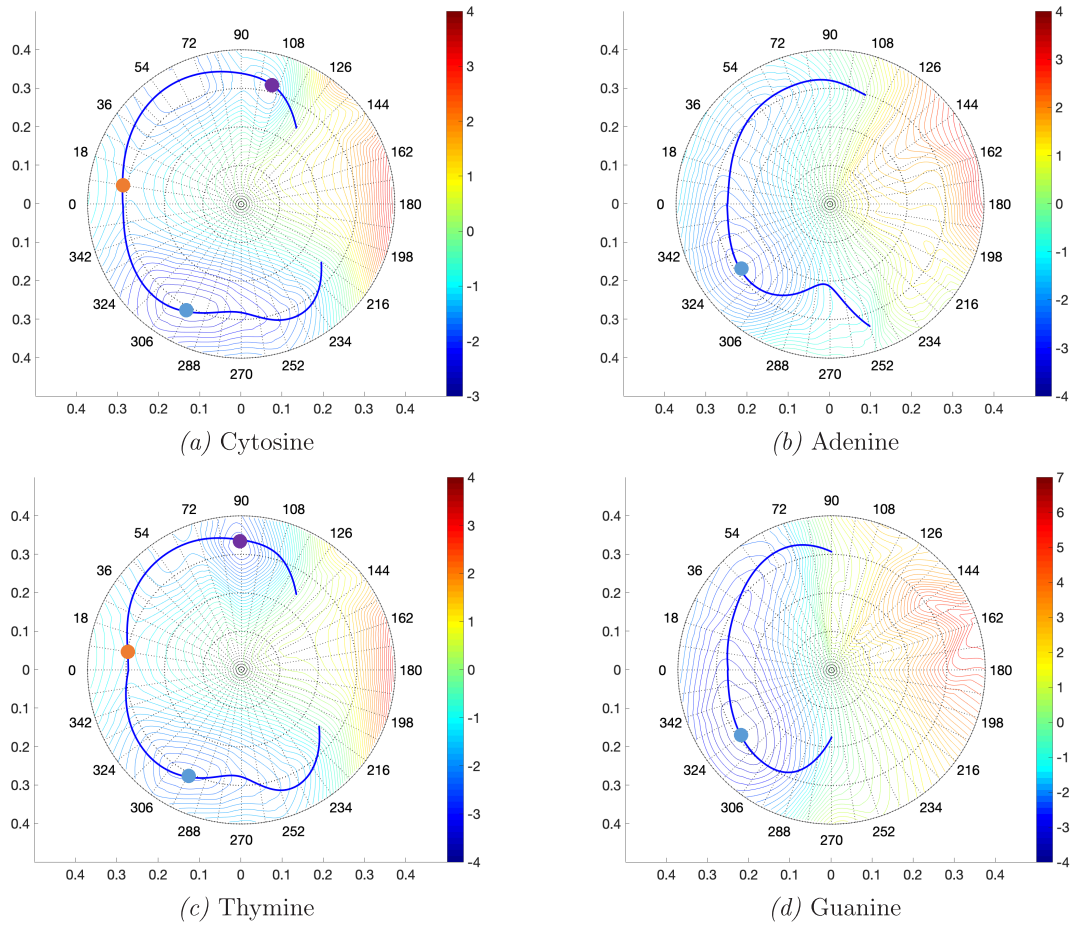

Figure 14. CESs and pseudolibration paths of the H-bond free deoxyribonucleosides **dCm** (a); **dAm** (b); **dTm** (c); and **dGm** (d). At the center of each CES, the planar deoxyribose ring form is located. The corresponding energy is used as reference. Both x and y axes show the magnitude of puckering amplitude q_2 in angstroms. The outer radius of the CES represents the maximum puckering amplitude of 0.4 Å. The labels around CES circle denote the value of the phase angle ϕ_2 in degrees. The solid blue line indicates the pseudolibration path. The color bar represents the energy on the CES in kilocalories per mole relative to the planar form: (*yellow to red regions*) location of conformers higher in energy than the planar form; (*green to blue regions*) location of conformers lower in energy than the planar form. The purple dot in the range 90−108° shows the location of the local, the blue dot near 306° the location of the global minimum, and the yellow dot near 9° the transition state between the two minima for **dCm** and **dTm**. The blue dot at 324° shows the single minimum for **dAm** and **dGm**. Calculated at the ωB97X-D/6-31++G(d,p) level of theory.

caused by ring inversion, i.e. the pseudorotation path is not a closed circle but an open curve, which we coined as a pseudolibration path. On each of the pseudolibration paths a global minimum in the range of ϕ_2 = 72°−90° and a local minimum in the range of ϕ_2 = 306° separated by a transition state in the range of ϕ_2 = 18°−342° could be identified. Harmonic frequency calculations identified all conformers in the global and local minimum regions as minimum structures (no imaginary frequency) and that in the transition region as a transition structure (one imaginary frequency). In this regard, the pseudorotation path can be considered as a special reaction path with the phase angle ϕ_2 as a reaction coordinate. Studies of H-bond free deoxyribonucleoside analogs revealed that removal of the H-bond does not restore the full conformational flexibility of the sugar ring. For all analogs there exists still a pseudolibration path, which for the pyrimidic bases is considerably longer compared with their original counterparts. This reflects that H-bonding invokes more strain on the pyrimidic bases than on the puric bases.

2. There are two major factors determining the conformational flexibility of the deoxyribonucleosides, ring puckering and internal H-bonding. Our work showed that ring puckering plays the dominant role. All deoxyribonuclesides feature the same deoxyribose ring puckering pattern, and strongest puckering occurs in the global minimum region (ϕ_2 = 72°−90°, q_2 values up to 0.35 Å), followed by the puckering in the local minimum region (ϕ_2 = 288°−306°, q_2 values up to 0.31 Å), while smallest puckering (q_2 = 0.15−0.18 Å) occurs in the transition region in the range of ϕ_2 = 324°−54°. This suggests that the larger the puckering amplitude, the lower the conformational energy. In contrast no direct correlation between conformational energy and H-bond strength could be found.
3. We quantitatively assessed the H-bond strength of all conformers along the pseudorotation paths via bond strength orders BSO n derived from local vibrational force constants. We found a direct correlation between H-bond strength and H-bond length. Longest and weakest H-bonds were found in the local minimum region for all deoxyribonuclesides, whereas shortest and strongest H-

DOI: 10.1021/acs.jpca.9b05452
J. Phys. Chem. A 2019, 123, 7087−7103

bonds were found outside both the global minimum region at the turning points of the pseudolibration paths, where the deoxyribonuclesides bounce back into the opposite path direction. These results clearly reveal that H-bonding determines the shape and length of the pseudolibration paths. In addition to the H-bond strength we evaluated the covalent/electrostatic character of the H- bonds applying the Cremer−Kraka criterion of covalent bonding. H-bonding in the puric bases has more covalent character whereas for the pyrimidic bases the character of the H-bond is more electrostatic.

4. The formation of the internal H-bond is affected by the mutual orientation of the CH_2OH group and the base which in turn is depends on the puckering mode. The influence of this orientation on the H-bond formation was quantified via (i) two dihedral angles describing the rotation of the CH_2OH group and the base perpendicular to the sugar ring and (ii) two angles describing the tilting of to the he CH_2OH group and the base relative to the center of the deoxyribose ring. We found that the tilting movement is more pronounced for the puric bases although they are more bulky than their pyrimidic counterparts. Overall, our analysis suggests that side group rotation is more important for H-bond formation. Besides geometric factors the strength of the H-bond also depends on the orientation and electron density distribution of the lone pair of the H-bond acceptor atom (N, respectively O). We assessed both via the delocalization energy ΔE_{del}(HB). With larger ΔE_{del}(HB) values corresponding stronger H-bonds were found along the pseudolibration paths for puric bases in line with our finding that H-bonding in the puric bases is of more covalent nature and that the global minimum conformation of **dG** has the strongest H-bond of all conformers investigated in this work with a BSO n value of 0.436, which is even stronger than the H-bond in the water dimer (BSO n = 0.360).

Currently, we are applying our new analysis to the DNA building blocks deoxyribonucleotides, which possess a more complex internal H-bonding pattern caused by the phosphate group, and to the characterization of unnatural base pairs which have recently drawn a lot of attention.[103,104]

■ ASSOCIATED CONTENT

Supporting Information

The Supporting Information is available free of charge on the ACS Publications website at DOI: 10.1021/acs.jpca.9b05452.

Cut through the CES of Adenine for a fixed value of the puckering phase angle ϕ_2. 3D plot of the CES for adenine. Geometries of **dA**, **dG**, **dC**, and **dT** at the global minimum, transition state, and local minimum (PDF)

■ AUTHOR INFORMATION

Corresponding Author

*E-mail: ekraka@smu.edu.

ORCID

Elfi Kraka: 0000-0002-9658-5626

Author Contributions

‡S.L. and N.B. contributed equally to this work.

Notes

The authors declare no competing financial interest.

■ ACKNOWLEDGMENTS

Dieter Cremer (1944−2017) originally suggested and established the framework for this work. We thank Wenli Zou for helpful discussions and suggestions. This work was financially supported by the National Science Foundation Grant CHE 1464906. We thank SMU for generous supercomputer resources.

■ REFERENCES

(1) Riccardi, C.; Musumeci, D.; Irace, C.; Paduano, L.; Montesarchio, D. Ru(III) Complexes for Anticancer Therapy: The Importance of Being Nucleolipidic. *Eur. J. Org. Chem.* **2017**, *2017*, 1100−1119.

(2) Kumar, V.; Kishor, S.; Ramaniah, L. M. Chemical Reactivity Analysis of Deoxyribonucleosides and Deoxyribonucleoside Analogues (NRTIs): A First-Principles Density Functional Approach. *J. Mol. Model.* **2012**, *18*, 3969−3980.

(3) Baker, D.; Chu, C. *Nucleosides and Nucleotides as Antitumor and Antiviral Agents*; Springer, 2013.

(4) Hocek, M. Synthesis of Base-Modified 2′-Deoxyribonucleoside Triphosphates and Their Use in Enzymatic Synthesis of Modified DNA for Applications in Bioanalysis and Chemical Biology. *J. Org. Chem.* **2014**, *79*, 9914−9921.

(5) Kielkowski, P.; Fanfrlík, J.; Hocek, M. 7-Aryl-7-deazaadenine 2′-Deoxyribonucleoside Triphosphates (dNTPs): Better Substrates for DNA Polymerases than dATP in Competitive Incorporations. *Angew. Chem., Int. Ed.* **2014**, *53*, 7552−7555.

(6) Raindlová, V.; Pohl, R.; Šanda, M.; Hocek, M. Direct Polymerase Synthesis of Reactive Aldehyde-Functionalized DNA and Its Conjugation and Staining with Hydrazines. *Angew. Chem., Int. Ed.* **2010**, *49*, 1064−1066.

(7) Morales, J. C.; Kool, E. T. Varied Molecular Interactions at the Active Sites of Several DNA Polymerases: Nonpolar Nucleoside Isosteres as Probes. *J. Am. Chem. Soc.* **2000**, *122*, 1001−1007.

(8) Škerlová, J.; Fábry, M.; Hubálek, M.; Otwinowski, Z.; Řezáčová, P. Structure of the Effector-Binding Domain of Deoxyribonucleoside Regulator DeoR from Bacillus Subtilis. *FEBS J.* **2014**, *281*, 4280−4292.

(9) Salleron, L.; Magistrelli, G.; Mary, C.; Fischer, N.; Bairoch, A.; Lane, L. DERA is the Human Deoxyribose Phosphate Aldolase and is Involved in Stress Response. *Biochim. Biophys. Acta, Mol. Cell Res.* **2014**, *1843*, 2913−2925.

(10) Horinouchi, N.; Ogawa, J.; Kawano, T.; Sakai, T.; Saito, K.; Matsumoto, S.; Sasaki, M.; Mikami, Y.; Shimizu, S. Biochemical Retrosynthesis of 2′-Deoxyribonucleosides from Glucose, Acetaldehyde, and a Nucleobase. *Appl. Microbiol. Biotechnol.* **2006**, *71*, 615−621.

(11) Honda, K.; Maya, S.; Omasa, T.; Hirota, R.; Kuroda, A.; Ohtake, H. Production of 2-deoxyribose 5-phosphate from Fructose to Demonstrate a Potential of Artificial Bio-Synthetic Pathway Using Thermophilic Enzymes. *J. Biotechnol.* **2010**, *148*, 204−207.

(12) Poole, A. M.; Horinouchi, N.; Catchpole, R. J.; Si, D.; Hibi, M.; Tanaka, K.; Ogawa, J. The Case for an Early Biological Origin of DNA. *J. Mol. Evol.* **2014**, *79*, 204−212.

(13) Altona, C.; Sundaralingam, M. Conformational Analysis of the Sugar Ring in Nucleosides and Nucleotides. New Description Using the Concept of Pseudorotation. *J. Am. Chem. Soc.* **1972**, *94*, 8205−8212.

(14) Szczepaniak, M.; Moc, J. Conformational Studies of Gas-Phase Ribose and 2-deoxyribose by Density Functional, Second Order PT and Multi-Level Method Calculations: The Pyranoses, Furanoses, and Open-Chain Structures. *Carbohydr. Res.* **2014**, *384*, 20−36.

(15) Taniguchi, T.; Nakano, K.; Baba, R.; Monde, K. Analysis of Configuration and Conformation of Furanose Ring in Carbohydrate and Nucleoside by Vibrational Circular Dichroism. *Org. Lett.* **2017**, *19*, 404−407.

(16) Li, L.; Szostak, J. W. The Free Energy Landscape of Pseudorotation in 3′-5′ and 2′-5′ Linked Nucleic Acids. *J. Am. Chem. Soc.* **2014**, *136*, 2858−2865.

(17) Shishkin, O. V.; Pelmenschikov, A.; Hovorun, D. M.; Leszczynski, J. Molecular Structure of Free Canonical 2′-Deoxyribo-

DOI: 10.1021/acs.jpca.9b05452
J. Phys. Chem. A 2019, 123, 7087−7103

nucleosides: A Density Functional Study. *J. Mol. Struct.* **2000**, *526*, 329−341.
(18) Wu, R. R.; Yang, B.; Frieler, C. E.; Berden, G.; Oomens, J.; Rodgers, M. T. N3 and O2 Protonated Tautomeric Conformations of 2′-Deoxycytidine and Cytidine Coexist in the Gas Phase. *J. Phys. Chem. B* **2015**, *119*, 5773−5784.
(19) Storoniak, P.; Rak, J.; Ko, Y. J.; Wang, H.; Bowen, K. H. Photoelectron Spectroscopic and Density Functional Theoretical Studies of the 2′-deoxycytidine Homodimer Radical Anion. *J. Chem. Phys.* **2013**, *139*, 075101.
(20) Ponomareva, A. G.; Yurenko, Y. P.; Zhurakivsky, R. O.; Van Mourik, T.; Hovorun, D. M. Complete Conformational Space of the Potential HIV-1 Reverse Transcriptase Inhibitors d4U and d4C. A Quantum Chemical Study. *Phys. Chem. Chem. Phys.* **2012**, *14*, 6787−6795.
(21) Tehrani, Z. A.; Javan, M. J.; Fattahi, A.; Hashemi, M. M. Structures, Stabilities & Conformational Behaviors of Hydrogen-Atom Abstractions of Cytosine Nucleosides: AIM & NBO Analysis. *Comput. Theor. Chem.* **2011**, *971*, 19−29.
(22) Matta, C. F.; Castillo, N.; Boyd, R. J. Extended Weak Bonding Interactions in DNA: π-Stacking (base-base), Base-Backbone, and Backbone-Backbone Interactions. *J. Phys. Chem. B* **2006**, *110*, 563−578.
(23) Hocquet, A.; Ghomi, M. The Peculiar Role of Cytosine in Nucleoside Conformational Behavior: Hydrogen Bond Donor Capacity of Nucleic Bases. *Phys. Chem. Chem. Phys.* **2000**, *2*, 5351−5353.
(24) Huang, M.; Giese, T. J.; Lee, T. S.; York, D. M. Improvement of DNA and RNA Sugar Pucker Profiles from Semiempirical Quantum Methods. *J. Chem. Theory Comput.* **2014**, *10*, 1538−1545.
(25) Cremer, D.; Pople, J. A. General Definition of Ring Puckering Coordinates. *J. Am. Chem. Soc.* **1975**, *97*, 1354−1358.
(26) Cremer, D. RING - A Coordinate Transformation Program for Evaluating the Degree and Type of Puckering of a Ring Compound. *Quantum Chem. Program Exchange* **1975**, *288*, 1−8.
(27) Cremer, D.; Pople, J. A. Molecular Orbital Theory of the Electronic Structure of Organic Compounds. XXIII. Pseudorotation in Saturated Five-Membered Ring Compounds. *J. Am. Chem. Soc.* **1975**, *97*, 1358−1367.
(28) Cremer, D. Theoretical Determination of Molecular Structure and Conformation. XI. the Puckering of Oxolanes. *Isr. J. Chem.* **1983**, *23*, 72−84.
(29) Essén, H.; Cremer, D. On the Relationship Between the Mean Plane and the Least-Squares Plane of an N-membered Puckered Ring. *Acta Crystallogr., Sect. B: Struct. Sci.* **1984**, *40*, 418−420.
(30) Cremer, D. Calculation of Puckered Rings with Analytical Gradients. *J. Phys. Chem.* **1990**, *94*, 5502−5509.
(31) Konkoli, Z.; Cremer, D. A New Way of Analyzing Vibrational Spectra I. Derivation of Adiabatic Internal Modes. *Int. J. Quantum Chem.* **1998**, *67*, 1−11.
(32) Konkoli, Z.; Cremer, D. A New Way of Analyzing Vibrational Spectra III. Characterization of Normal Vibrational Modes in Terms of Internal Vibrational Modes. *Int. J. Quantum Chem.* **1998**, *67*, 29−41.
(33) Konkoli, Z.; Larsson, J. A.; Cremer, D. A New Way of Analyzing Vibrational Spectra II. Comparison of Internal Mode Frequencies. *Int. J. Quantum Chem.* **1998**, *67*, 11−29.
(34) Konkoli, Z.; Larsson, J. A.; Cremer, D. A New Way of Analyzing Vibrational Spectra IV. Application and Testing of Adiabatic Modes within the Concept of the Characterization of Normal Modes. *Int. J. Quantum Chem.* **1998**, *67*, 41−55.
(35) Bader, R. F. W.; Slee, T. S.; Cremer, D.; Kraka, E. Description of Conjugation and Hyperconjugation in Terms of Electron Distributions. *J. Am. Chem. Soc.* **1983**, *105*, 5061−5068.
(36) Cremer, D.; Kraka, E.; Slee, T. S.; Bader, R. F. W.; Lau, C. D. H.; Dang, T. T. N.; MacDougall, P. J. Description of Homoaromaticity in Terms of Electron Distributions. *J. Am. Chem. Soc.* **1983**, *105*, 5069−5075.
(37) Geise, H. J.; Adams, W. J.; Bartell, L. S. Electron Diffraction Study of Gaseous Tetrahydrofuran. *Tetrahedron* **1969**, *25*, 3045−3052.
(38) McQuarrie, D. A. *Statistical Thermodynamics*; Harper & Row: New York, 1973.
(39) Luger, P.; Buschmann, J. Twist Conformation of Tetrahydrofuran in the Crystal. *Angew. Chem., Int. Ed. Engl.* **1983**, *22*, 410−410.
(40) David, W. I. F.; Ibberson, R. M.; Dennis, T. J. S.; Hare, J. P.; Prassides, K. Structural Phase Transitions in the Fullerene C_{60}. *Europhys. Lett.* **1992**, *18*, 219−225.
(41) Han, S. J.; Kang, Y. K. Pseudorotation in Heterocyclic Five-membered Rings: Tetrahydrofuran and Pyrrolidine. *J. Mol. Struct.: THEOCHEM* **1996**, *369*, 157−165.
(42) Wu, A.; Cremer, D. New Approach for Determining the Conformational Features of Pseudorotating Ring Molecules Utilizing Calculated and Measured NMR Spin-Spin Coupling Constants. *J. Phys. Chem. A* **2003**, *107*, 1797−1810.
(43) Lambert, J. B.; Papay, J. J.; Khan, S. A.; Kappauf, K. A.; Magyar, E. S. Conformational Analysis of Five-membered Rings. *J. Am. Chem. Soc.* **1974**, *96*, 6112−6118.
(44) Kalinowski, H. O.; Berger, S.; Braun, S. *^{13}C-NMR-Spektroskopie [13 hoch C-NMR-Spektroskopie]: 200 Tabellen*; Thieme, 1984.
(45) Wilson, G. M. Vapor-Liquid Equilibrium. XI. A New Expression for the Excess Free Energy of Mixing. *J. Am. Chem. Soc.* **1964**, *86*, 127−130.
(46) Zou, W.; Kalescky, R.; Kraka, E.; Cremer, D. Relating Normal Vibrational Modes to Local Vibrational Modes With the Help of an Adiabatic Connection Scheme. *J. Chem. Phys.* **2012**, *137*, 084114.
(47) Zou, W.; Cremer, D. Properties of Local Vibrational Modes: The Infrared Intensity. *Theor. Chem. Acc.* **2014**, *133*, 1451−1466.
(48) Zou, W.; Kalescky, R.; Kraka, E.; Cremer, D. Relating Normal Vibrational Modes to Local Vibrational Modes: Benzene and Naphthalene. *J. Mol. Model.* **2013**, *19*, 2865−2877.
(49) Zou, W.; Cremer, D. C_2 in a Box: Determining its Intrinsic Bond Strength for the $X^1\Sigma_g^+$ Ground State. *Chem. - Eur. J.* **2016**, *22*, 4087−4089.
(50) Kraka, E.; Setiawan, D.; Cremer, D. Re-evaluation of the Bond Length-Bond Strength Rule: The Stronger Bond is Not Always the Shorter Bond. *J. Comput. Chem.* **2016**, *37*, 130−142.
(51) Setiawan, D.; Kraka, E.; Cremer, D. Hidden Bond Anomalies: The Peculiar Case of the Fluorinated Amine Chalcogenides. *J. Phys. Chem. A* **2015**, *119*, 9541−9556.
(52) Kalescky, R.; Kraka, E.; Cremer, D. Identification of the Strongest Bonds in Chemistry. *J. Phys. Chem. A* **2013**, *117*, 8981−8995.
(53) Humason, A.; Zou, W.; Cremer, D. 11, 11-Dimethyl-1, 6-methano[10]annulene - An Annulene with an Ultralong CC Bond or a Fluxional Molecule? *J. Phys. Chem. A* **2015**, *119*, 1666−1682.
(54) Kalescky, R.; Zou, W.; Kraka, E.; Cremer, D. Quantitative Assessment of the Multiplicity of Carbon-Halogen Bonds: Carbenium and Halonium Ions with F, Cl, Br, I. *J. Phys. Chem. A* **2014**, *118*, 1948−1963.
(55) Kraka, E.; Cremer, D. Characterization of CF Bonds with Multiple-Bond Character: Bond Lengths, Stretching Force Constants, and Bond Dissociation Energies. *ChemPhysChem* **2009**, *10*, 686−698.
(56) Kalescky, R.; Kraka, E.; Cremer, D. New Approach to Tolman's Electronic Parameter Based on Local Vibrational Modes. *Inorg. Chem.* **2014**, *53*, 478−495.
(57) Setiawan, D.; Kalescky, R.; Kraka, E.; Cremer, D. Direct Measure of Metal-Ligand Bonding Replacing the Tolman Electronic Parameter. *Inorg. Chem.* **2016**, *55*, 2332−2344.
(58) Cremer, D.; Kraka, E. Generalization of the Tolman Electronic Parameter: The Metal-Ligand Electronic Parameter and the Intrinsic Strength of the Metal-Ligand Bond. *Dalton T.* **2017**, *46*, 8323−8338.
(59) Li, Y.; Oliveira, V.; Tang, C.; Cremer, D.; Liu, C.; Ma, J. The Peculiar Role of the Au_3 Unit in Au_m Clusters: σ-Aromaticity of the Au_5Zn^+ Ion. *Inorg. Chem.* **2017**, *56*, 5793−5803.
(60) Kalescky, R.; Kraka, E.; Cremer, D. Description of Aromaticity with the Help of Vibrational Spectroscopy: Anthracene and Phenanthrene. *J. Phys. Chem. A* **2014**, *118*, 223−237.
(61) Setiawan, D.; Kraka, E.; Cremer, D. Quantitative Assessment of Aromaticity and Antiaromaticity Utilizing Vibrational Spectroscopy. *J. Org. Chem.* **2016**, *81*, 9669−9686.

DOI: 10.1021/acs.jpca.9b05452
J. Phys. Chem. A 2019, 123, 7087−7103

(62) Oliveira, V.; Kraka, E.; Cremer, D. Quantitative Assessment of Halogen Bonding Utilizing Vibrational Spectroscopy. *Inorg. Chem.* **2017**, *56*, 488−502.
(63) Oliveira, V.; Kraka, E.; Cremer, D. The Intrinsic Strength of the Halogen Bond: Electrostatic and Covalent Contributions Described by Coupled Cluster Theory. *Phys. Chem. Chem. Phys.* **2016**, *18*, 33031−33046.
(64) Oliveira, V.; Cremer, D. Transition from Metal-Ligand Bonding to Halogen Bonding Involving a Metal as Halogen Acceptor a Study of Cu, Ag, Au, Pt, and Hg Complexes. *Chem. Phys. Lett.* **2017**, *681*, 56−63.
(65) Setiawan, D.; Kraka, E.; Cremer, D. Strength of the Pnicogen Bond in Complexes Involving Group Va Elements N, P, and As. *J. Phys. Chem. A* **2015**, *119*, 1642−1656.
(66) Setiawan, D.; Kraka, E.; Cremer, D. Description of Pnicogen Bonding With the Help of Vibrational Spectroscopy - The Missing Link Between Theory and Experiment. *Chem. Phys. Lett.* **2014**, *614*, 136−142.
(67) Setiawan, D.; Cremer, D. Super-Pnicogen Bonding in the Radical Anion of the Fluorophosphine Dimer. *Chem. Phys. Lett.* **2016**, *662*, 182−187.
(68) Tao, Y.; Zou, W.; Jia, J.; Li, W.; Cremer, D. Different Ways of Hydrogen Bonding in Water - Why Does Warm Water Freeze Faster than Cold Water? *J. Chem. Theory Comput.* **2017**, *13*, 55−76.
(69) Freindorf, M.; Kraka, E.; Cremer, D. A Comprehensive Analysis of Hydrogen Bond Interactions Based on Local Vibrational Modes. *Int. J. Quantum Chem.* **2012**, *112*, 3174−3187.
(70) Kalescky, R.; Zou, W.; Kraka, E.; Cremer, D. Vibrational Properties of the Isotopomers of the Water Dimer Derived from Experiment and Computations. *Aust. J. Chem.* **2014**, *67*, 426−434.
(71) Kalescky, R.; Zou, W.; Kraka, E.; Cremer, D. Local Vibrational Modes of the Water Dimer - Comparison of Theory and Experiment. *Chem. Phys. Lett.* **2012**, *554*, 243−247.
(72) Kalescky, R.; Kraka, E.; Cremer, D. Local Vibrational Modes of the Formic Acid Dimer - The Strength of the Double Hydrogen Bond. *Mol. Phys.* **2013**, *111*, 1497−1510.
(73) Zhang, X.; Dai, H.; Yan, H.; Zou, W.; Cremer, D. B-H···π Interaction: A New Type of Nonclassical Hydrogen Bonding. *J. Am. Chem. Soc.* **2016**, *138*, 4334−4337.
(74) Kraka, E.; Freindorf, M.; Cremer, D. Chiral Discrimination by Vibrational Spectroscopy Utilizing Local Modes. *Chirality* **2013**, *25*, 185−196.
(75) Kraka, E.; Larsson, J. A.; Cremer, D. *Computational Spectroscopy: Methods, Experiments and Applications*; Wiley-VCH Verlag GmbH and Co. KGaA, 2010; pp 105−149.
(76) Bader, R. F. W. Atoms in Molecules. *Acc. Chem. Res.* **1985**, *18*, 9−15.
(77) Bader, R. *Atoms in Molecules: A Quantum Theory*; International Series of Monographs on Chemistry; Clarendon Press: Oxford, 1990.
(78) Cremer, D.; Kraka, E. Chemical Bonds without Bonding Electron Density? Does the Difference Electron-Density Analysis Suffice for a Description of the Chemical Bond? *Angew. Chem., Int. Ed. Engl.* **1984**, *23*, 627−628.
(79) Cremer, D.; Kraka, E. A Description of the Chemical Bond in Terms of Local Properties of Electron Density and Energy. *Croat. Chem. Acta* **1984**, *57*, 1259−1281.
(80) Kraka, E.; Cremer, D. *Theoretical Models of Chemical Bonding. The Concept of the Chemical Bond*; Maksic, Z. B., Ed.; Springer Verlag: Heidelberg, 1990; Vol. 2, p 453.
(81) Reed, A.; Curtiss, L.; Weinhold, F. Intermolecular Interactions from A Natural Bond Orbital, Donor-Acceptor Viewpoint. *Chem. Rev.* **1988**, *88*, 899−926.
(82) Weinhold, F.; Landis, C. R. *Valency and Bonding: A Natural Bond Orbital Donor-Acceptor Perspective*; Cambridge University Press, 2003.
(83) Weinhold, F. Natural Bond Critical Point Analysis: Quantitative Relationships Between Natural Bond Orbital-Based and QTAIM-Based Topological Descriptors of Chemical Bonding. *J. Comput. Chem.* **2012**, *33*, 2440−2449.
(84) Zhang, Z.; Li, D.; Jiang, W.; Wang, Z. The Electron Density Delocalization of Hydrogen Bond Systems. *Adv. Phys.* **2018**, *3*, 298−315.
(85) Chai, J. D.; Head-Gordon, M. Long-Range Corrected Hybrid Density Functionals with Damped Atom-Atom Dispersion Corrections. *Phys. Chem. Chem. Phys.* **2008**, *10*, 6615−6620.
(86) Chai, J. D.; Head-Gordon, M. Systematic Optimization of Long-Range Corrected Hybrid Density Functionals. *J. Chem. Phys.* **2008**, *128*, 084106.
(87) Hehre, W. J.; Ditchfield, R.; Pople, J. A. Self-Consistent Molecular Orbital Methods. XII. Further Extensions of Gaussian-Type Basis Sets for Use in Molecular Orbital Studies of Organic Molecules. *J. Chem. Phys.* **1972**, *56*, 2257−2261.
(88) Ditchfield, R.; Hehre, W. J.; Pople, J. A. Self-Consistent Molecular-Orbital Methods. IX. An Extended Gaussian-Type Basis for Molecular-Orbital Studies of Organic Molecules. *J. Chem. Phys.* **1971**, *54*, 724−728.
(89) Clark, T.; Chandrasekhar, J.; Spitznagel, G. W.; Schleyer, P. V. R. Efficient Diffuse Function-Augmented Basis Sets for Anion Calculations. III. The 3-21+G Basis Set for First-Row Elements, Li−F. *J. Comput. Chem.* **1983**, *4*, 294−301.
(90) Frisch, M. J.; Pople, J. A.; Binkley, J. S. Self-Consistent Molecular Orbital Methods 25. Supplementary Functions for Gaussian Basis Sets. *J. Chem. Phys.* **1984**, *80*, 3265−3269.
(91) Gräfenstein, J.; Cremer, D. Efficient Density-Functional Theory Integrations by Locally Augmented Radial Grids. *J. Chem. Phys.* **2007**, *127*, 164113.
(92) Frisch, M. J.; Trucks, G. W.; Schlegel, H. B.; Scuseria, G. E.; Robb, M. A.; Cheeseman, J. R.; Scalmani, G.; Barone, V.; Mennucci, B.; Petersson, G. A. et al. *Gaussian 09*, Revision B.1; Gaussian, Inc.: Wallingford, CT, 2010.
(93) Kraka, E.; Cremer, D.; Filatov, M.; Zou, W.; Grafenstein, J.; Izotov, D.; Gauss, J.; He, Y.; Wu, A.; Polo, V. et al. *COLOGNE2019*; Southern Methodist University: Dallas, TX, 2019.
(94) Glendening, E. D.; Badenhoop, J. K.; Reed, A. E.; Carpenter, J. E.; Bohmann, J. A.; Morales, C. M.; Landis, C. R.; Weinhold, F. *NBO6*; Theoretical Chemistry Institute, University of Wisconsin: Madison, 2013.
(95) Keith, T. *TK Gristmill Software*; Overland Park, KS, USA, 2011; see http://aim.tkgristmill.com.
(96) Kraka, E.; Cremer, D. Weaker Bonds with Shorter Bond Lengths. *Rev. Proc. Quim.* **2012**, *6*, 31.
(97) Kraka, E.; Setiawan, D.; Cremer, D. Re-Evaluation of the Bond Length-Bond Strength Rule: The Stronger Bond is not Always the Shorter Bond. *J. Comput. Chem.* **2016**, *37*, 130−142.
(98) Cremer, D. *Modelling of Structure and Properties of Molecules*; Maksic, Z. B., Ed.; Ellis Horwood: Chichester, 1987; p 125.
(99) Freindorf, M.; Kraka, E.; Cremer, D. A Comprehensive Analysis of Hydrogen Bond Interactions Based on Local Vibrational Modes. *Int. J. Quantum Chem.* **2012**, *112*, 3174−3187.
(100) Kalescky, R.; Zou, W.; Kraka, E.; Cremer, D. Vibrational Properties of the Isotopomers of the Water Dimer Derived from Experiment and Computations. *Aust. J. Chem.* **2014**, *67*, 426−434.
(101) Tao, Y.; Zou, W.; Kraka, E. Strengthening of Hydrogen Bonding with the Push-Pull Effect. *Chem. Phys. Lett.* **2017**, *685*, 251−258.
(102) Herbert, H. E.; Halls, M. D.; Hratchian, H. P.; Raghavachari, K. Hydrogen-Bonding Interactions in Peptide Nucleic Acid and Deoxyribonuclei Acid: A Comparative Study. *J. Phys. Chem. B* **2006**, *110*, 3336−3343.
(103) Eremeeva, E.; Herdewijn, P. Non Canonical Genetic Material. *Curr. Opin. Biotechnol.* **2019**, *57*, 25−33.
(104) Hoshika, S.; Leal, N. A.; Kim, M.-J.; Kim, M.-S.; Karalkar, N. B.; Kim, H.-J.; Bates, A. M.; Watkins, N. E., Jr.; SantaLucia, H. A.; Meyer, A. J.; et al. Hachimoji DNA and RNA: A Genetic System with Eight Building Blocks. *Science* **2019**, *363*, 884−887.

DOI: 10.1021/acs.jpca.9b05452
J. Phys. Chem. A 2019, 123, 7087−7103